UNIVERSITÀ POLITECNICA DELLE MARCHE

FACOLTÀ DI INGEGNERIA

Corso di Laurea Magistrale in

BIOMEDICAL ENGINEERING

METHODS FOR NON-CONTACT MEASUREMENT OF RESPIRATORY AND CARDIAC RATE

Supervisor :

Prof. Lorenzo Scalise

Co-Supervisor:

Ing. Luca Antognoli

Thesis Written By:

TAYE NZALI Delluc Steve

Accademic Year 2019/2020

Table of Contents

ACKNOWLEDGMENT

All praise and thanks to Almighty God, the most merciful, most gracious, most gifted source of knowledge and wisdom in mankind, who has given us the power of the spirit and the ability to lead to well this project in the exciting ocean of knowledge.

I would like to express my gratitude to the director of this study, **Professor Lorenzo Scalise** for his efforts and guidance throughout this study and for inspiring and motivating me to achieve the goal and co-supervising **Engineer Luca Antognoli** for his help and advice at the start of this laboratory study, which allowed me to work with passion on this study.

I would like to thank my family who have always supported me especially my father who has always been present. I would like to dedicate this study to my mother who died fourteen years ago today, but still present in spirit.

I would like to express my gratitude to all my friends for the support at every stage passed over the past two years and during which we have gone through the good times and the hard times.

In the end, I would like to thank everyone who supported me and helped me anyway during my stay here in Ancona in Italy and who helped to make this endeavor happen.

Thank you all.

LIST OF FIGURES

Figure 23: The flowchart of the proposed FSR system.

Figure 24: The received signal of the FSR system with a different orientation angle α for (a) 0°; (b) 30°; (c) 60°; (d) 90°; (e) the received signal of the FSR system with nobody in the test area.

Figure 25: The output of the envelope detection with the different orientation angle α for (a) 0°; (b) 30°; (c) 60°; and (d) 90°.

Figure 26: The comparison between FSR and PVDF (polyvinylidene fluoride) with the different orientation angle α for (a) 0°; (b) 90°.

Figure 27: Acquisition and processing of the IR-UWB radar signals from the heart. (A) The experiment was conducted with participants whose clothes were on after 5–10 minutes' rest. (B) The IR-UWB radar system transmitted radiofrequency pulse waves and received signals reflected from an object. (C) The raw signals passed through a bandpass filter to cancel noise, then were processed to separate clutter signals from target signals.

Figure 28: Examples of the heart signal waveforms obtained from the IR-UWB radar. The agreements between the radar and ECG were grossly excellent in both the healthy volunteers with NSR (A) and the patients with AF (B). The red dots indicate the same time points on both the radar waveform and ECG.

Figure 29: Heart rate monitoring system using microwave Doppler sensor and range imagery.

Figure 30: Doppler sensor output with body motion artifact

Figure 31: Gain adjustment of Doppler signal with body motion artifact.

Figure 32: Measurement result of heart rate extraction and comparison with reference sensor and conventional method.

Figure 33: (a) the experimental setup; (b) the annotated photograph of the proposed monitoring system.

Figure 34: Schematic diagram of the proposed monitoring system.

Figure 35: The breathing signal obtained by the reference system (upper trace) and the breathing signal obtained by the proposed monitoring system (lower trace).

Figure 36: Principles of measuring heart rate using infrared/RGB facial-image analysis.

Figure 37: Experimental protocol.

Figure 38: Heartbeat curves obtained from ECG and visible images. The heartbeat signal obtained from RGB camera.

Figure 39: Schematic representation of the experimental set-up used to monitor the beating of the heart: (a) red low-power laser diode, (b) fibre optic bundle, (c) germanium photodiode, (d) water receptacle, (e) hydraulic device to position the mollusc, (f) the oyster and (g) the data acquisition–monitoring system.

Figure 40: Waveform of the heartbeat of an oyster (a) surrounded by air and (b) in salt water. Depicted is the variation with time of the voltage measured in the photodiode.

Figure 41: Signal from an oyster immersed in salt water. The signal has three parts. The high frequency fluctuations correspond to the beating of the heart, the modulations with maxima around 40, 80 and 110 s are related to the movement of the gills while the high peaks around 25, 60 and 95 s are identified with the sudden closing of the valves.

Figure 42: Distribution of the time interval between heartbeats, as obtained from the time difference between two peaks associated with the contraction of the ventricle. The distribution was computed from a 6 h recording.

LIST OF TABLES

In many clinical situations, monitoring respiration is a necessity. This is especially true when treating patients with respiratory problems in intensive care unit, patients with skin trouble from attached sensor, burn and the unconscious avoiding the need to apply electrodes and to wire the subject to the monitor.

This literature review includes published works that have been peer-reviewed. Our search was mainly focused on articles in journals, chapters of periodicals and proceedings of conferences written in English published between 2000 and 2020. We firstly searched on Google Scholar search engine with key words ‘respiratory rate’, ‘respiration rate’, ‘breathing rate’, ‘tachypnea’, or ‘apnea’, in combination with ‘measurement’, ‘monitoring’, ‘detection’, ‘estimation’, ‘wearable devices’, or ‘extraction’. More than 800 papers were found. From the titles of the works, technical keywords were extracted including electrocardiogram (ECG), photoplethysmogram (PPG), radar, thermal imaging, and others.

The main parameters to evaluate the quality of breathing are the respiration rate, the amplitude of the single respiration acts (Max to Min) and in some cases the shape of the measured signal, regularity and irregularity, respectively.

This document present different methods to measure respiration and heart rate and show the result on different graph

INTRODUCTION

Respiration monitoring is among the most important elements of assessing the physiological state. Given that nearly 5% of the total human population suffers from respiration illnesses such as Sleep Apnea Syndrome (SAS) and about 30% of people in their seventies are reported to have a respiration disease in industrially developed countries [1], effective methods for monitoring respiration is essential. According to the World Health Organization (WHO), the top five respiratory diseases account for 17.4% of all deaths and 13.3% of all Disability-Adjusted Life Years (DALYs) [1]. Lower respiratory tract infections, Chronic Obstructive Pulmonary Disease (COPD), tuberculosis and lung cancer are each among the 10 leading causes of death worldwide.

Breathing is one of the essential functions for the survival of most living beings. Many processes to measure the respiration rate have been proposed: using a stretch sensor or impedance meter to detect chest expansion, a pulse oximeter and extracting the respiration rate from the raw data, an accelerometer to detect chest expansion and contraction, measuring airflow pressure by oral or nasal cannula, and many others. In case of sleep apnea diagnosis for example, polysomnography (PSG), the commonly used test, employs nasal cannula and chest belts. The main problem common to all these techniques is the presence of a device directly in contact with the subject. As an example, for children this may induce rejection behavior leading them to remove the device. This is also true in the case of sleeping subjects, where the presence of the device can significantly disrupt the falling asleep and sleep.

There have been several studies on non-contact respiration measurement methods through the observation of body surface movement changes with respiration. The **laser monitor** measures the distance between the chest wall and the sensor and obtains a respiratory waveform by plotting the change in distance over time, the **electromagnetic waves** can sense chest movement by Doppler effect or by analyzing the signal backscattered by breathing movements and **ultrasound waves** telemeters permits detection of small body displacements during respiration.

In this study, the non-contact methods for respiratory monitoring proposed in the last years have been based on the working principle:

- Electromagnetic sensors
- Laser
- Ultrasounds
- Optical sensor

This has allowed us to explore the potential for using non-contact sensor to serve as an inexpensive method for long-term respiration monitoring.

I- CARDIO-RESPIRATORY SYSTEM

The job of the respiratory system is transporting oxygen from the air we breathe, through a system of tubes, into our lungs. This is then diffused into the bloodstream, whilst carbon dioxide makes the opposite journey and exits our body.

The cardiorespiratory system is consisting of the heart and blood vessels. These work in tandem with the respiratory system, which consist of the lungs as well as airways. These two-body systems transport oxygen to the muscles and organs of the body. In addition, they remove waste products, such as carbon dioxide.

1- Respiratory system

The Process of breathing is an important and vital aspects of life according to definition, the breathing is the process of respiration, in which air is inhaled into lungs via mouth or nose due to muscle contraction and then exhaled due to muscle relaxation. The Physiology of breathing consist of very sophisticated process that allows the diffusion of oxygen (O2) into blood and carbon dioxide (CO2) from blood to the external environment.

The upper respiratory tract begins at the nose and runs down to the nasopharynx, oropharynx and the larynx. The function the conducting airways is to filter, warm and humidify inspired gases.

The lower respiratory tract begins with the trachea at the level of C6 and extends to T4 where it bifurcates into the right and left main bronchi, lobar bronchi, segmental bronchi and terminal and respiratory bronchioles leading to the alveolar ducts and sacs. The respiratory bronchioles, alveolar ducts and sacs are the sites of gas exchange [34].

Breathing or pulmonary ventilation is the increase of alveolar pressure created by inspiration, where the thorax expands by the movement of the rib cage equally and bilaterally upwards and outwards by the external intercostal muscles. At the same time the diaphragm, the other main breathing muscle, contracts downwards; this reduces the pressure within the lungs to less than that of the atmosphere and therefore draws air into them. Expiration is the relaxation of the intercostal and diaphragm muscles and the expelling of the oxygen and carbon dioxide [34].

Respiratory rate or the number of breaths per minute is defined as one breath to each movement of air in and out of the lungs. In general, the respiratory rate for an adult sits between 12 and 20 breaths per minute, but there will be some variation depending on age and medical condition. An increase or decrease in the respiratory rate indicates the requirement for more or less oxygen or carbon dioxide in the body. It is accepted that a respiratory rate of above 25 breaths per minute or an increasing respiratory rate can indicate that a patient could be deteriorating. A reduction in respiratory rate to 8 or fewer breaths per minute is also indicative of patient deterioration. The significance of this assessment should not be underestimated because ineffective breathing negatively impacts on effective gas exchange [34].

Respiratory rate measurement is termed as a core nursing skill. Respiratory rate is a non-invasive and useful assessment tool and abnormalities in respiratory rate have been shown to indicate patient deterioration and should be managed accordingly. Changes and anomalies in respiratory rate are not simply associated with respiratory condition they are a good indicator that a patient is struggling to maintain homeostatic control (the body's internal environment). Respiratory rate is an early, extremely good indicator of physiological conditions such as hypoxia (low levels of oxygen in the cells), hypercapnia (high levels of carbon dioxide in the bloodstream), metabolic and respiratory acidosis.

CONDITION	CHANGES IN BREATHING
Pleural Effusion	Dyspnoea—difficulty breathing
Pneumothorax	Asymmetrical chest expansion Use of accessory muscles
Exacerbation of asthma	Dyspnoea—difficulty breathing, wheeze Tachypnoea—raised respiratory rate above 20 breaths per minute
Exacerbation of chronic obstructive pulmonary disease	Dyspnoea—difficulty breathing, wheeze Tachypnoea—raised respiratory rate above 20 breaths per minute

Table 1: Examples of conditions that lead to abnormal breathings.

Good observation of respiratory rate provides the opportunity to incidences of severe illness and improve the clinical response for patients [34].

Below are the points that are listed some aspects of monitoring the respiration and their significance:

- The ideal observation of respiratory rate takes into consideration the importance of how the person is breathing, as well as the rate at which they are breathing.
- Respiratory rate, depth and symmetry are indicative of different types of condition.
- The ideal length of time to take a respiratory rate measurement continues to be 1 minute (60 seconds) (Flenady et al, 2017)—without patient awareness that they are being monitored (Hill et al, 2018)
- Respiratory rate changes all the time to adjust to the body's homeostatic balance; evidence suggests that reduced length of monitoring will reduce the number of breaths measured and thus the likelihood of indication that the patient is becoming unwell.
- Oxygen saturation measurement is not a replacement for respiratory rate measurement.
- Accurate documentation and interpretation of accurately taken observations help improve patient outcomes.

Thus, a respiratory rate is a vital sign used to monitor the progression of illness and an abnormal respiratory rate is an important marker of serious illness. There is substantial evidence that alterations in respiratory rate can be used to predict potentially serious clinical events such as cardiac arrest or admission to the intensive care unit.

The calculation and analysis of the displacement of chest wall during breathing is an important aspect of monitoring. In clinical practice, respiratory function is generally evaluated using spirometry and physical examinations. Spirometry is useful for quantitative assessments of lung volume and flow and can be objectively compared with other spirometric results. Physical examinations, such as inspection and palpation of respiratory function, provide real-time observations and do not require a special measuring instrument; thus, they are important components of assessments in clinical settings [35].

The respiratory movement measuring instrument, which consists of 6 laser distance sensors, has been developed to measure changes in breathing movements of the thorax and abdomen. However, it is limited to measuring the anteroposterior diameters of breathing movements. Although several previous studies have assessed the 3-dimensional motions of the thorax and abdomen during breathing using infrared cameras and an electromagnetic device, there is no reported literature on the 3-dimensional distances of the observational points on the thorax and abdomen during breathing [35].

After reading previous studies that calculated the chest wall displacement it is reported that in an adult the maximum displacement is not more than 5mm in the case of deep breathing [36]. The study calculated movement specific to regions, for S1-2 regions during inspiration 3-5mm displacement was reported in cranial direction while in the lateral direction the movement is smaller about 1-2mm [36].

2- Cardiac system

The job of the circulatory system is to carry blood, nutrients as well as waste throughout the body. The circulatory system consists of three autonomous systems which function together:

- The heart (cardiovascular),
- Lungs (pulmonary),
- Arteries, veins, coronary as well as portal vessels (systemic).

This system is responsible for the flow of blood, nutrients, oxygen, other gases in addition to hormones to and from cells.

In the circulatory system, the heart is functions as a pump. To be specific, the heart is a double pump. What we mean by this is that blood which requires oxygen comes into the heart and is pumped by the first pump into the lungs. The second pump of the heart pushes the oxygen rich blood to all the other sections of the body. This gives the heart its usual lub-dub sound.

The lungs work together with the circulatory system in order to pump oxygen rich blood to all of the cells in your body. After this, the blood collects carbon dioxide, as well as other waste products and transports these back to the lungs. Here, these are pumped out of the body when we breathe out.

The number of times that the heart pumps, or beats, is measured in a minute. This is known as a person’s pulse rate and this is affected by their current activity level:

- If you are sleeping, or doing no physical activity at all, your heart is pumping at a resting heart rate.
- When you are active, you are making use of all your body systems which need fuel in the form of calories (which are found in food) and oxygen (which you breathe).

The more physical activity you do, the more fuel your muscles require. For this reason, your breathing rate as well as your heart rate increase when you take part in exercise. Having the knowledge of how to take your own heart rate can assist you with exercising properly as well as safely.

It is possible to take your own heart rate by finding two major blood vessels, or arteries, on your body. These two blood vessels are described as radial and carotid:

- The radial artery is located on the inside of your wrist near the side of your thumb.
- The carotid artery is found on your neck between your windpipe and neck muscles, as well as just under your lower jawbone.

Locate your pulse using both your index and middle fingers. Count the pulses, or beats, for 10 seconds.

Heart rate is the speed of the heartbeat measured by the number of contractions (beats) of the heart per minute (bpm). The heart rate can vary according to the body's physical needs, including the need to absorb oxygen and excrete carbon dioxide, but is also modulated by a myriad of factors including but not limited to genetics, physical fitness, stress or psychological status, diet, drugs, hormonal status, environment, and disease/illness as well as the interaction between and among these factors. It is usually equal or close to the pulse measured at any peripheral point.

The American Heart Association states the normal resting adult human heart rate is 60–100 bpm. Tachycardia is a high heart rate, defined as above 100 bpm at rest. Bradycardia is a low heart rate, defined as below 60 bpm at rest. During sleep a slow heartbeat with rates around 40–50 bpm is common and is considered normal. When the heart is not beating in a regular pattern, this is referred to as an arrhythmia. Abnormalities of heart rate sometimes indicate disease.

Increased metabolic by products associated with increased activity, such as carbon dioxide, hydrogen ions, and lactic acid, plus falling oxygen levels, are detected by a suite of chemoreceptors innervated by the glossopharyngeal and vagus nerves. These chemoreceptors provide feedback to the cardiovascular centers about the need for increased or decreased blood flow, based on the relative levels of these substances.

The limbic system can also significantly impact HR related to emotional state. During periods of stress, it is not unusual to identify higher than normal HRs, often accompanied by a surge in the stress hormone cortisol. Individuals experiencing extreme anxiety may manifest panic attacks with symptoms that resemble those of heart attacks. These events are typically transient and treatable. Meditation techniques have been developed to ease anxiety and have been shown

to lower HR effectively. Doing simple deep and slow breathing exercises with one's eyes closed can also significantly reduce this anxiety and HR [36].

FACTOR	EFFECT
Cardioaccelerator nerves	Release of norepinephrine
Proprioreceptors	Increased rates of firing during exercise
Chemoreceptors	Decreased levels of O_2; increased levels of H^+, CO_2, and lactic acid
Baroreceptors	Decreased rates of firing, indicating falling blood volume/pressure
Limbic system	Anticipation of physical exercise or strong emotions
Catecholamines	Increased epinephrine and norepinephrine
Thyroid hormones	Increased T3 and T4
Calcium	Increased Ca^{2+}
Potassium	Decreased K^+
Sodium	Decreased Na^+
Body temperature	Increased body temperature
Nicotine and caffeine	Stimulants, increasing heart rate

Table 2: Major factors increasing heart rate and force of contraction.

Using a combination of auto rhythmicity and innervation, the cardiovascular center is able to provide relatively precise control over the heart rate, but other factors can impact on this. These include hormones, notably epinephrine, norepinephrine, and thyroid hormones; levels of various ions including calcium, potassium, and sodium; body temperature; hypoxia; and pH balance.

The heart rate can be slowed by altered sodium and potassium levels, hypoxia, acidosis, alkalosis, and hypothermia. The relationship between electrolytes and HR is complex but maintaining electrolyte balance is critical to the normal wave of depolarization. Of the two ions, potassium has the greater clinical significance. Initially, both hyponatremia (low sodium levels) and hypernatremia (high sodium levels) may lead to tachycardia. Severely high hypernatremia may lead to fibrillation, which may cause CO to cease. Severe hyponatremia leads to both bradycardia and other arrhythmias. Hypokalemia (low potassium levels) also leads to arrhythmias,

whereas hyperkalemia (high potassium levels) causes the heart to become weak and flaccid, and ultimately to fail.

Heart muscle relies exclusively on aerobic metabolism for energy. Severe (an insufficient supply of oxygen) leads to decreasing HRs, since metabolic reactions fueling heart contraction are restricted.

FACTOR	EFFECT
Cardioinhibitor nerves (vagus)	Release of acetylcholine
Proprioreceptors	Decreased rates of firing following exercise
Chemoreceptors	Increased levels of O_2; decreased levels of H^+ and CO_2
Baroreceptors	Increased rates of firing, indicating higher blood volume/pressure
Limbic system	Anticipation of relaxation
Catecholamines	Decreased epinephrine and norepinephrine
Thyroid hormones	Decreased T3 and T4
Calcium	Decreased Ca^{2+}
Potassium	Increased K^+
Sodium	Increased Na^+
Body temperature	Decrease in body temperature

Table 3: Factors decreasing heart rate and force of contraction.

II- METHOD FOR RESPIRATORY RATE

1- Ultrasounds

- **Measurement system**

The figure shows a non-contact respiration measurement system block diagram. It consists of an ultrasonic sensor module, MP150 data acquisition module (BIOPAC™, USA), signal processing module and a personal computer. Each of the test results was acquired through a BIOPAC™ MP150 with a 1 kHz sampling rate, which was saved in a PC using MATLAB™ version 7 as the data analysis tool. The analogue output of the ultrasonic sensor was transferred to the personal computer through a MP150 module [2].

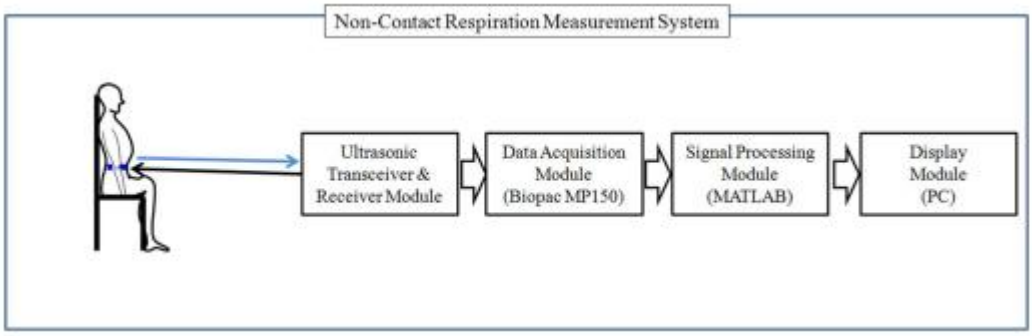

Figure1: Block diagram of noncontact respiration measurement system.

- **Experimental setup**

The measurement distance is set at 100 cm in the sitting position. The ultrasonic sensor is approximately at level with the subject's abdomen area. A nasal thermocouple sensor (TP-TSD202A, BIOPAC™) is used for comparison with non-contact respiration system. The nasal thermocouple sensor was affixed on the subject's nose. Experiment duration is 180 s. The experimental procedure is shown in Table below. The subject was asked to remain still and refrain from scratching, talking, and any other motion for the duration of each measurement if possible.

Posture	Measurement distance (cm)	Cloth	Measuring time (min)
Sit on chair	100	On	3
		Break time	
		Off	3

Table 4: Experimental protocol

To verify the amount of abdominal circumference, change during subjects' respiration, the abdominal circumference in inhale (ACI) and abdominal circumference in exhale (ACE) were

measured. It is assumed that circumference changes with abdominal respiration are enough to detect with ultrasonic sensor, which has 0.3 mm spatial resolution [2].

- **Results**

The signals following the modified enveloped detection were filtered by using the moving average and the peak of the signal detected by zero crossing methods to classify respiration rate, as shown in Figures 2 and 3. Figure 2 is the output signal of the subject without clothes and Fig. 3 is the signal from the same subject with clothes on. The upper panels in both Figures 2(a) and 3(a) are the nasal thermocouple output signals after moving average filtering, while the bottom panels are the ultrasonic sensor output after moving average filtering. The results from peak detection algorithm are shown in Figures 2(b) and 3(b). The number of detected peaks for subject using the ultrasonic sensor is 32, which is the same as the number of peaks observed using the nasal thermocouple sensor.

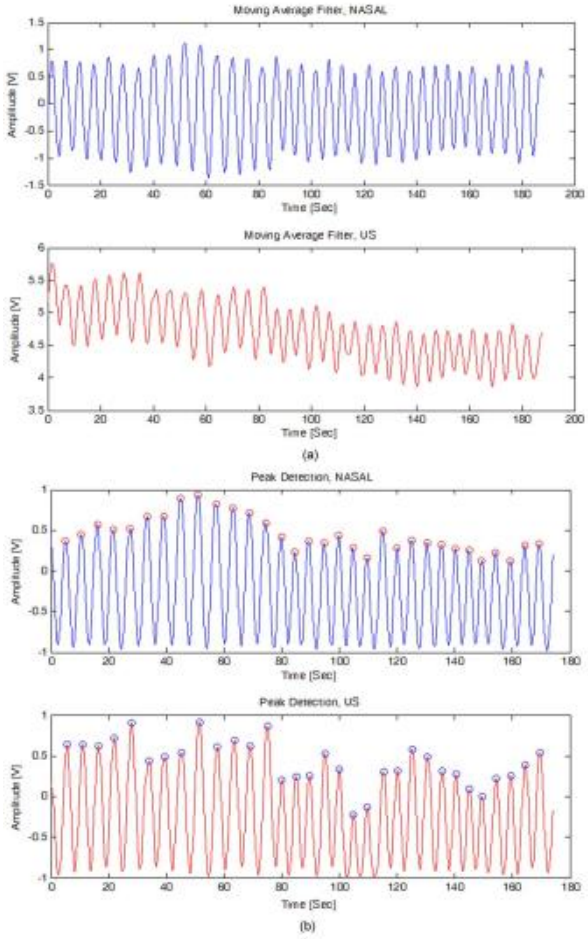

Figure 2: (a) The output signal from moving average filtering and (b) peak detected signal from subject without cloth on.

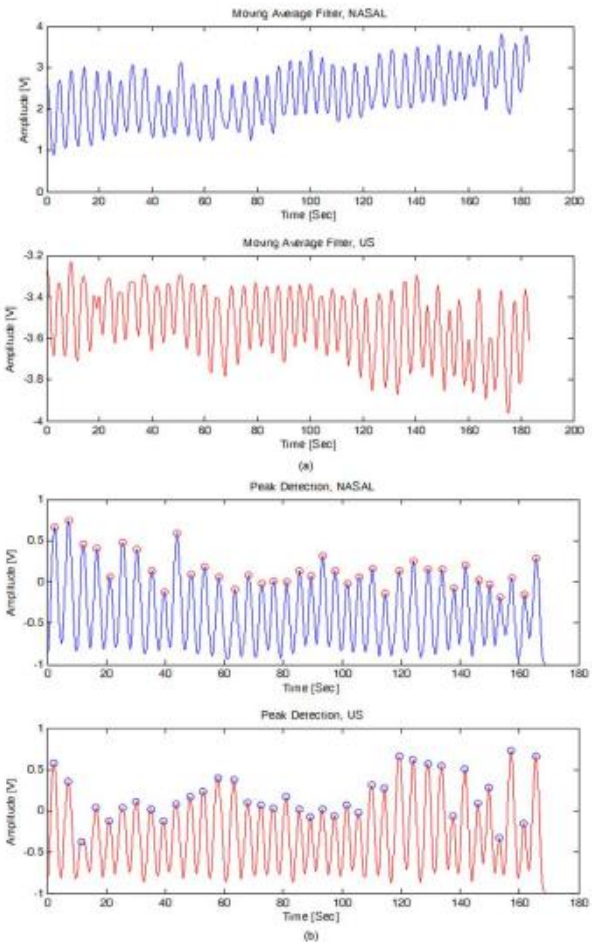

Figure 3: (a) The output signal from moving average filtering and (b) peak detected signal from subject with cloth on.

From subject, we compared both calculated respiration rates from the two sensors, as shown in Figure 4. The comparison of the respiration rates from unclothed surface is shown in Figure 4(a), while the respiration rates from clothed surface are shown in Figure 4(b). In both panels, a solid line represents the signal from the nasal thermocouple sensor and a dotted line represents the signal from the ultrasonic sensor. Throughout the duration of the experiment, respiration rates from each measurement method showed similar rates [2].

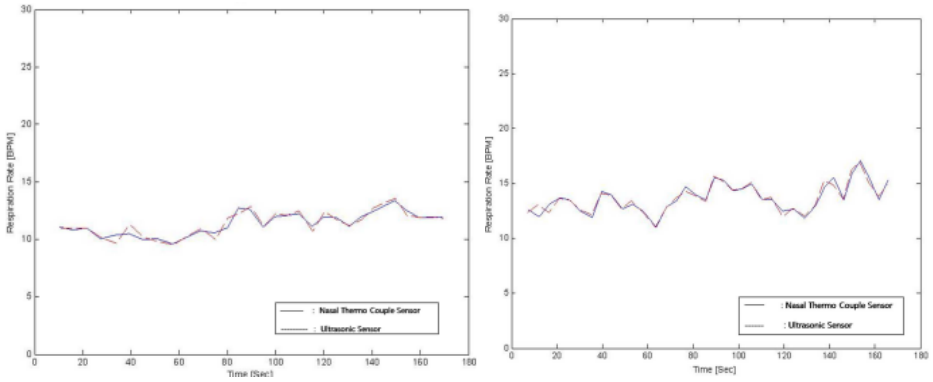

Figure 4: The comparison of respiration rate (RR), (a) RR comparison without cloth on, (b) RR comparison with cloth on.

The results of our experiment showed that the system can be used for respiration monitoring of patients. However, it is thought that the system could not detect enough body motion information for monitoring of the subject with a quilt or a thick blanket. With further improvements and investigation in the sensor for the enhancement of detection accuracy in any circumstances of the subject, the measurement range and the realization of real-time detection algorithm and diagnosis-assistance algorithm, we expect that the system can be used in early diagnosis of cardiorespiratory sleep disorders. Furthermore, by combining the system with available information and communication technologies (ICT), important data can be sent to medical experts in real time when a patient is suffering from such a disorder. In this way, this system can be applied to remote healthcare and mobile healthcare applications.

2- IR-UWB

- **Measurement system**

The experiments were conducted at the bedside in the NICU. The radar chip was covered with a white plastic cap. The radar system was hung at the end of a specially designed arm on a tripod and placed at a distance of 35 cm orthogonal to the chest [4]. The neonates were placed in a supine position inside an open-air crib, and the torso of the neonates was covered with a blanket. The experiment was planned to last as long as the baby was stable. The neonates were not touched or repositioned during the data collection, but clinical workflow always took priority over the recordings. The data collected from the radar were processed and stored in a laptop computer placed nearby [4]. To measure RR using IP (Impedance Pneumography), a BSM-6501K patient monitor (Nihon Kohden, Tokyo, Japan) was used. IP records changes in the electrical impedance of the patient's thorax. Three transcutaneous electrodes were attached at the standard positions, and a pulse oximetry sensor was placed on the sole of the neonates. An RR was calculated from the last eight waveforms, recorded on a memory card every second

and extracted using viewer software (BSM Viewer, Nihon Kohden, Tokyo, Japan). These RR values were averaged every 10 s for comparison with the radar results.

IR-UWB radar device (X4M06; Xandar Kardian, Delaware, USA) was used to send and collect the radar signals to and from the chest. The IR-UWB radar sensor is capable of detecting objects using the ultrawideband frequency band without interference from other sensors and measuring the distance to the objects. The radar module used has a centre frequency of 7.29 GHz and a bandwidth of 1.5 GHz. MATLAB, which is a commercially available software package, was used for acquiring, processing and storing the data. Signal processing was automatically performed by a software algorithm [3-5], and RR activity was isolated from the heartbeat signal by an algorithm described in another study [4,8].

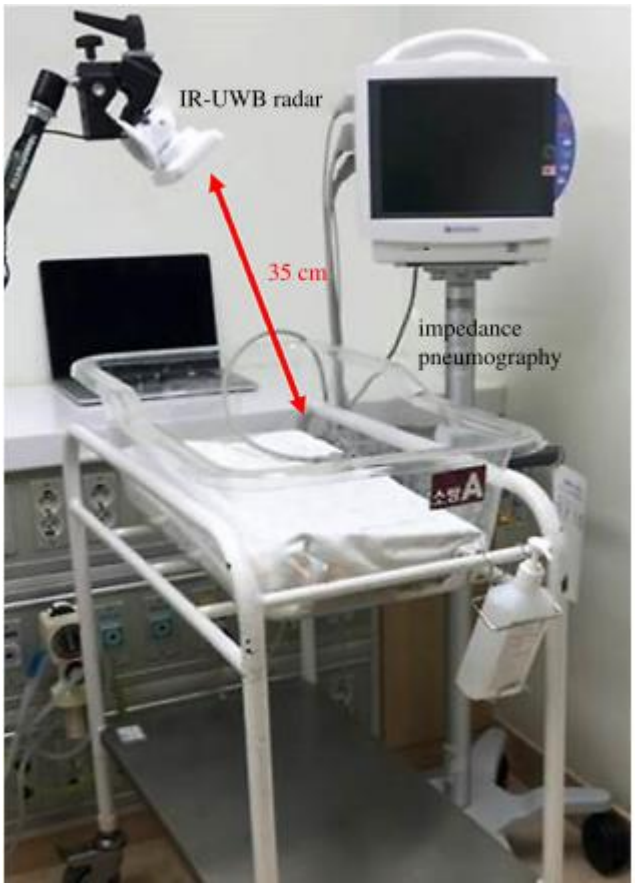

Figure 5: Experimental set-up for simultaneous IR-UWB radar and IP recording.

- **Experimental setup**

The block diagram of the IR-UWB radar signal processing flow for extraction of respiratory signals. Not only the signal from the target (newborn baby) to be observed, but also other surrounding background signals are received every second. Primarily, the unwanted clutter signal must be removed from the raw signal, and the next step is to combine those waveforms, resulting in a better frequency resolution for the vital sign. Because this extracted signal also includes breathing, heartbeat, motion and noise, the measurement noise is reduced by applying the Kalman filter estimation to the time-varying signal, and the range of the radar sensor is configurable through parameter frame stitches. The degree of motion from the extracted signal is integrated with the respiratory waveform; then, the fast Fourier

transform algorithm is applied to the constructed vital signal to find the respiratory signal frequency band.

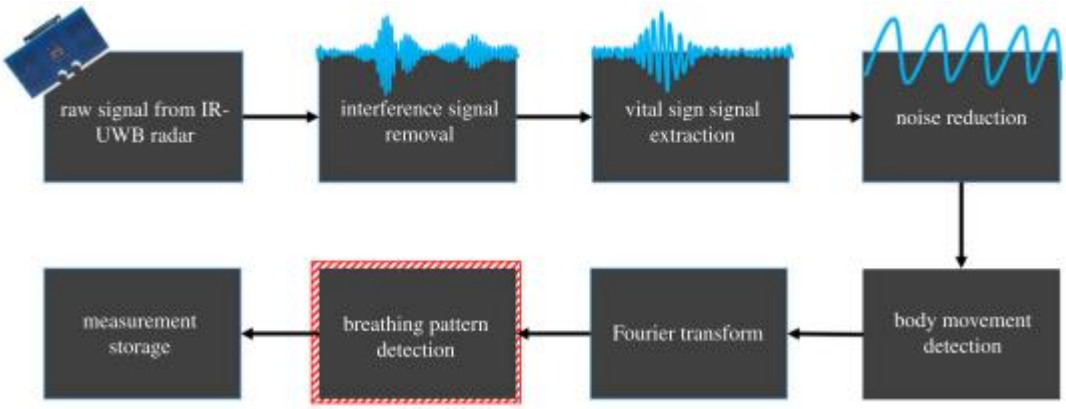

Figure 6: Block diagram of the IR-UWB radar signal processing flow for extraction of respiratory signals.

A Fourier transform decomposed a signal with respect to time into a frequency component was used to extract the frequency component of the RR from the vital sign signal. Figure 7 shows how the frame received by radar is processed as the algorithm progresses for each step in the diagram. The raw data are an unprocessed frame received from the radar, and the clutter removal signal is extracted by removing unwanted background signals received by the radar. In frames received dozens of times per second, the position of the infant can be extracted along the time axis to find a signal containing the respiratory wave.

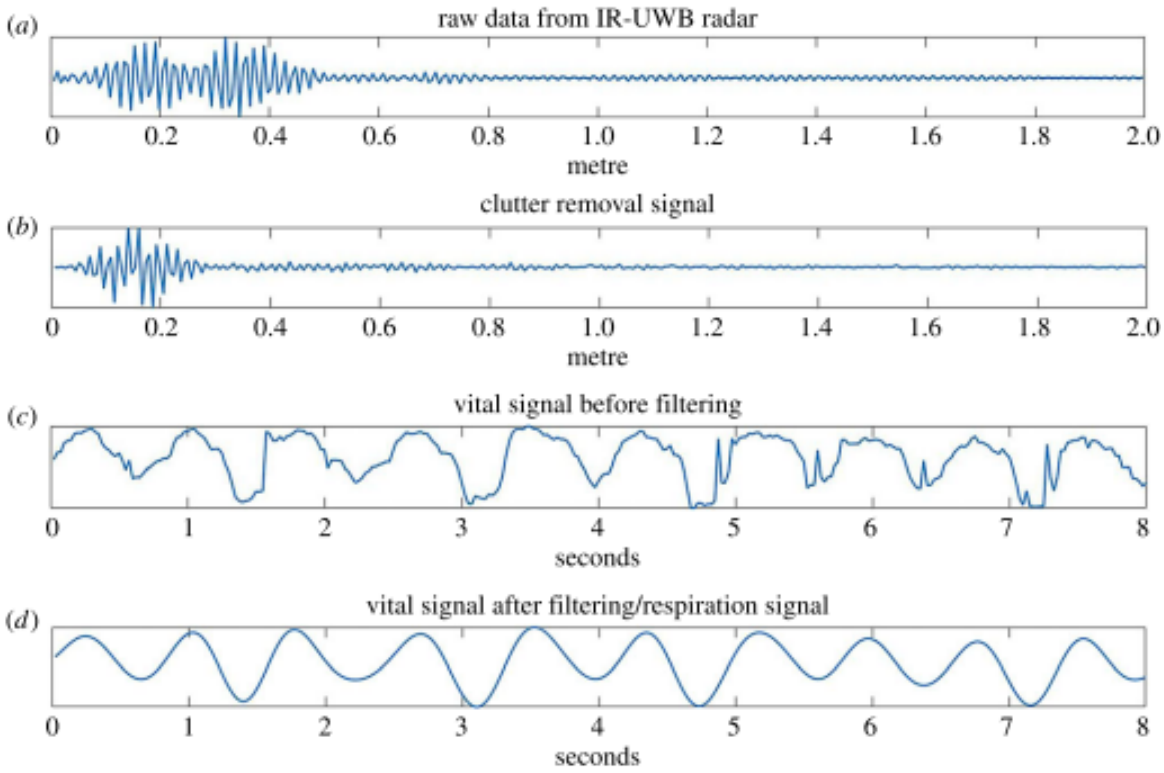

Figure 7: Radar signal obtained from each step of the block diagram. (a) Raw frame received by radar antenna. (b) Clutter removal frame obtained from background subtraction. (c) Neonatal respiratory waveform acquired for 8 s. (d) Respiratory waveform obtained through low pass filtering of neonatal respiration frequency.

- **Results**

The radar recordings were made within the unmodified environment of the NICU. The respiratory signal waveforms from IR-UWB radar appeared to correspond cycle by cycle to the IP waveform. When the intervals between breathing cycles were irregular and even an apnea cycle was presented, the crests and troughs of the respiratory signals from the IR-UWB radar also appeared to be well matched to the IP respiratory signals (figure 8a). Through synchronization of the two data streams, a representative case of measured RRs from both devices in a 5 min period is displayed in figure 8b. The absolute values and the change patterns of RRs are similar between the two devices; when the neonates moved, the discrepancies between the two RRs appeared to increase. The average recording duration of both the IR-UWB and IP was 134.3 min (range 100–160 min) [4]. The data that were obtained when the electrodes were detached from the neonates or when the neonates required feeding, diaper changes or any medical attentions (36% of the total measurement duration) were excluded from the analysis because RR IP was not recognized during these times. RRs were estimated every 10 s in both measurement methods.

By transmitting and receiving a band of radio waves, the IR-UWB radar system can recognize the patient's chest movements during breathing at a distance [14]. Due to its ultrawide bandwidth, the radar can penetrate the patient's clothing or blankets and extract the respiratory signals with high resolution. Because radar is not affected by the status of ambient lights or by the patient's skin colour, it can be used in a nursery even at night when the lights should be dim or off. The measurement system can be located at a more flexible range of distances from the subject with the radar method than with other non-contact vital sign monitoring methods. Compared to other devices, IR-UWB radar sensors typically have small sizes and simple structures, which would provide advantages in installation and operation of such devices.

Our results have shown that IR-UWB radar could accurately measure RRs in neonates in a non-contact manner. Although movements affected the agreement between the radar and IP measurements, the accuracy was still sufficiently high, even for high levels of movement. The radar was also easily applicable in the NICU environment, where the various surrounding instruments might interfere with the measurements and where the device itself could be an obstacle against daily neonatal care by physicians and nurses.

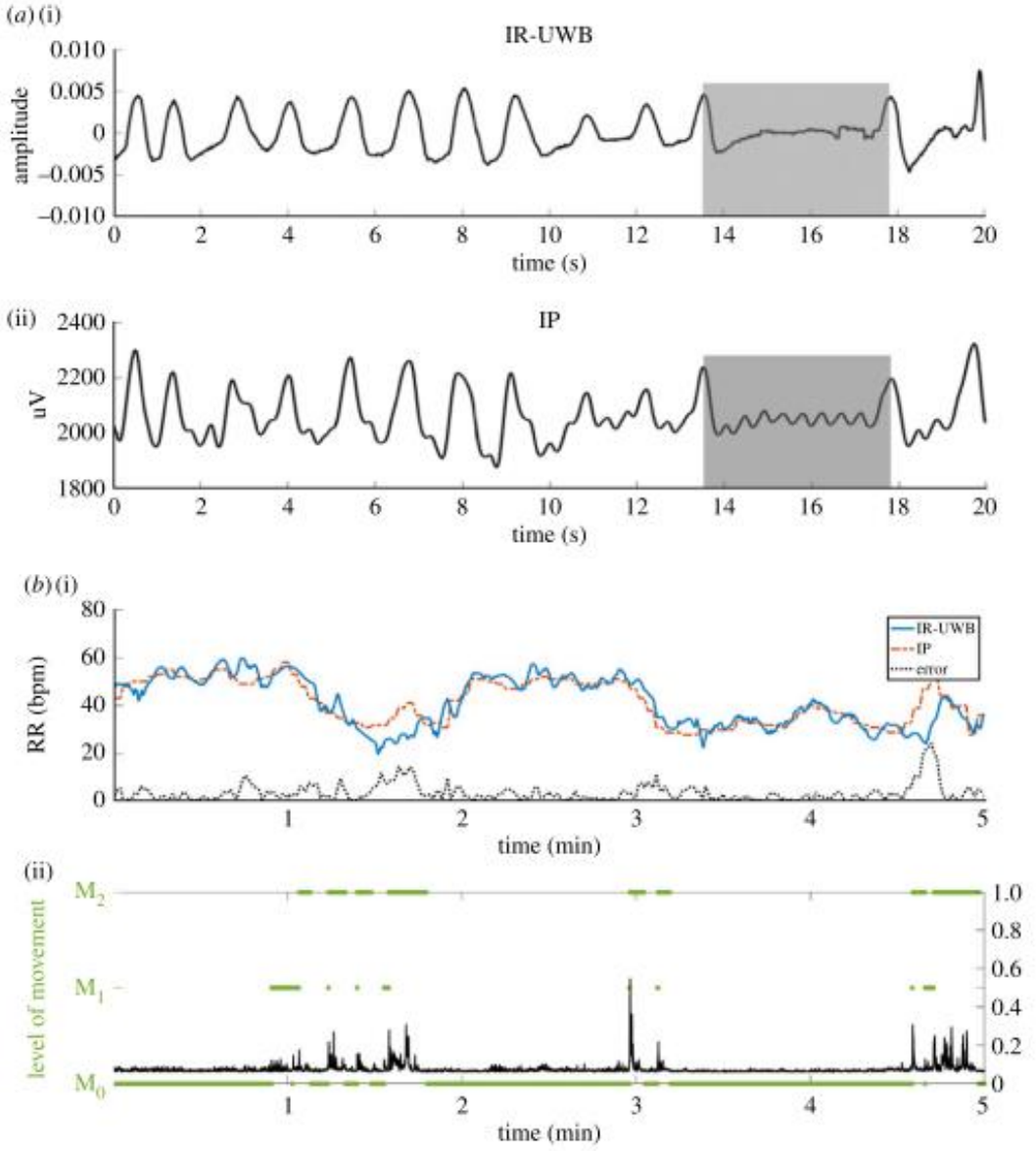

Figure 8: Representative results of the raw signal waveform and estimated RRs from both devices.

3- Laser

- **Measurement system and experimental setup**

To perform the test, first the phantom simulator was designed and operated using arduino board to provide with controlled breathing rate.

Figure 9 shows the scheme for the phantom acquisition [15]. The phantom was placed at 1m from LDV. The LDV was interfaced using ADI instruments card to the dedicated software of Lab Chart. the data is then exported to for further analysis using MATLAB software.

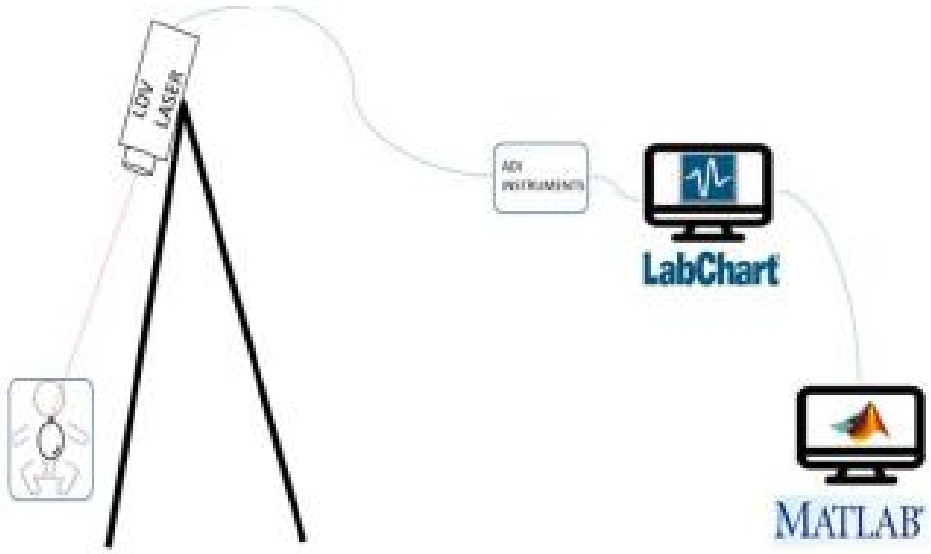

Figure 9: Scheme of phantom simulator

The subjects were asked to sit in upright position facing the LDV, The LDV sampling frequency is 1000Hz that is sufficient for the detection of breathing signal. The subjects were asked to simulate the conditions of apnea by holding there breath and conditions hyper and hypo respiration, figure 10 shows sheme of simulation [15].

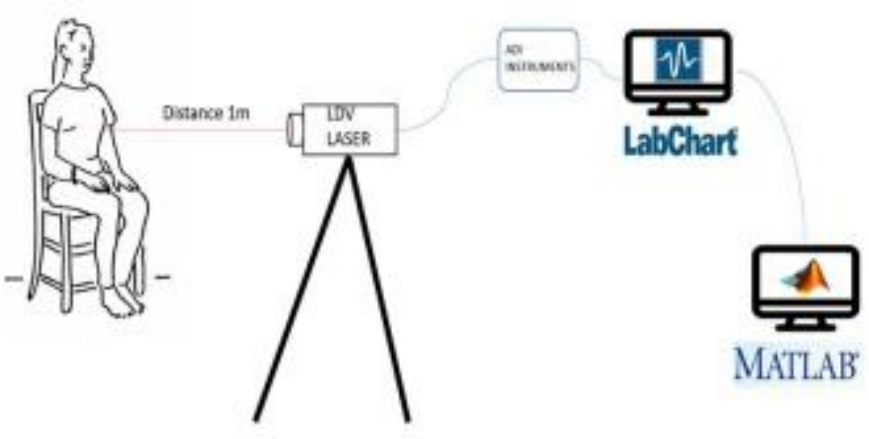

Figure 10: Scheme of human subject

The raw data that is acquired using LDV is exported to MATLAB for the analysis. The data was subjected to filter to remove all the noises. After noise removal a function is used to detect the breathing activity using variable percentile values. First the analysis is done using manual setting of parameters then the same data is fed to an algorithm that was designed as standard for all the runs of the tests.

The breathing event is detected, an algorithm is designed to further detect the conditions of Hyper, Hypo-respiration and Apnea. MATLAB is used to design GUI, this GUI allows user to

set the variable ranges for Hyper and Hypo respiration, also to set the percentile values that is helpful in detecting breathing events.

Figure 11: Normal Breathing Followed by Fast Breathing

- **Results**

Figure 12 represents GUI designed to simulate the pre-acquired signal in real time scenarios. It is capable to display 3 graphs, the main graph shows the chest wall movement that was derived from the velocity data, as LDV calculates velocity of chest wall movement. GUI also calculates the breathing tachogram, then the user can know instantaneous breathing rate, the third graph of GUI shows you the mean breathing rate calculated after every 30 seconds. This GUI app allows user to export data, define values for Hypo and Hyper respiration along with the percentile values that detects the breathing event. There are indicators that turn red if any of the danger situation happens, in this case that is slow breathing, High Breathing and Apnea.

This table shows the result of comparison between manual analysis of signal by visualizing and analysis through standardised algorithm designed for GUI for all the signals. As it is shown for different breathing rates provided controllably to the phantom using arduino board, the error is very low. By seeing the trend of error, it can be concurred that for higher breathing rates, the error percentage increases [15].

Provided Breathing Rate (BPM)	Results of Manual Analysis (BPM)	Results of Application Analysis of Signals (BPM)	Error Percentage %
20	20	19.8	1
40	39.9	39.7	0.5
60	59.2	57.2	3.4
80	78.2	78.4	0.2
100	98.6	97.6	1
120	116.6	112.6	3.4

Table 5: Result of comparison between manual analysis and analysis through standardised algorithm.

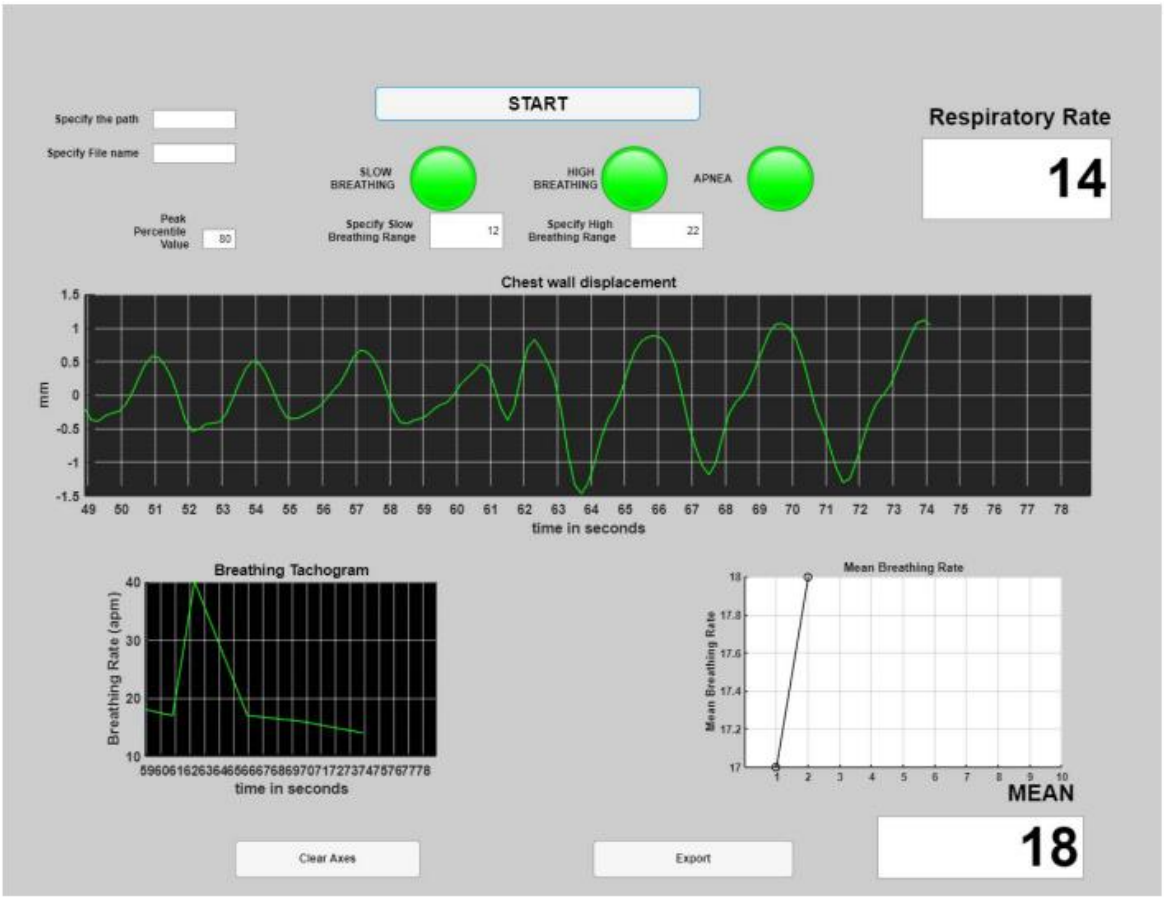

Figure 12: Graphical User Interface

The original signal acquired from the subject is shown in figure 13. The normal breathing signal is followed by the fast-breathing signal. This signal is acquired after performing the analysis through app with standardised algorithm. The Red Markers are indicating the detection of breathing event. In figure 14 the original signal acquired from the subject is acquired that shows the apnea condition is followed by hypo respiration.

The algorithm can detect no breathing even when there are very less chest wall movement is recorded. While when the subject was asked to perform deep breathing, the chest wall displacement is large with width between the peaks is wider than that of breathing conditions.

This algorithm can detect Apnea condition, the Hyper and Hypo respiration conditions. The GUI allows user to define the value for the detection of breathing event, along with the selection of ranges for Hyper and Hypo breathing conditions.

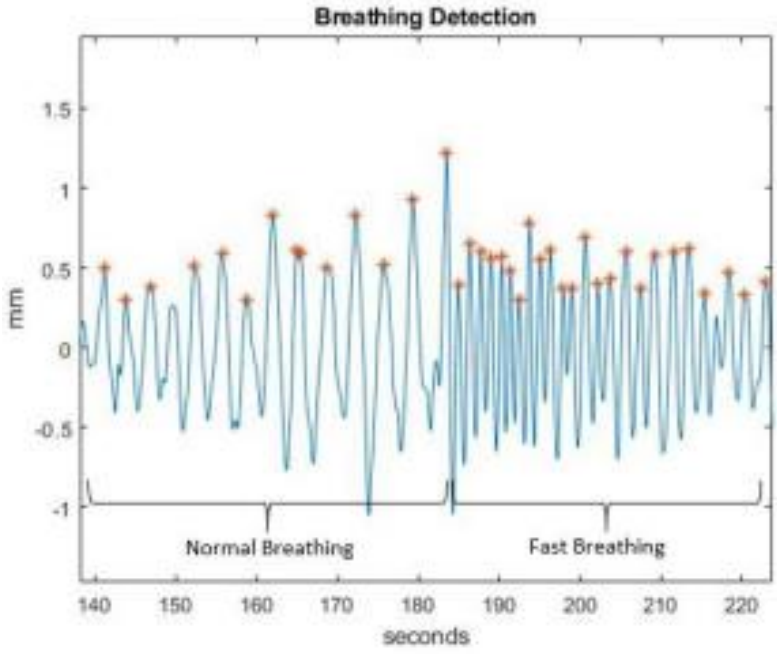

Figure 13: Normal Breathing followed by Hyper breathing.

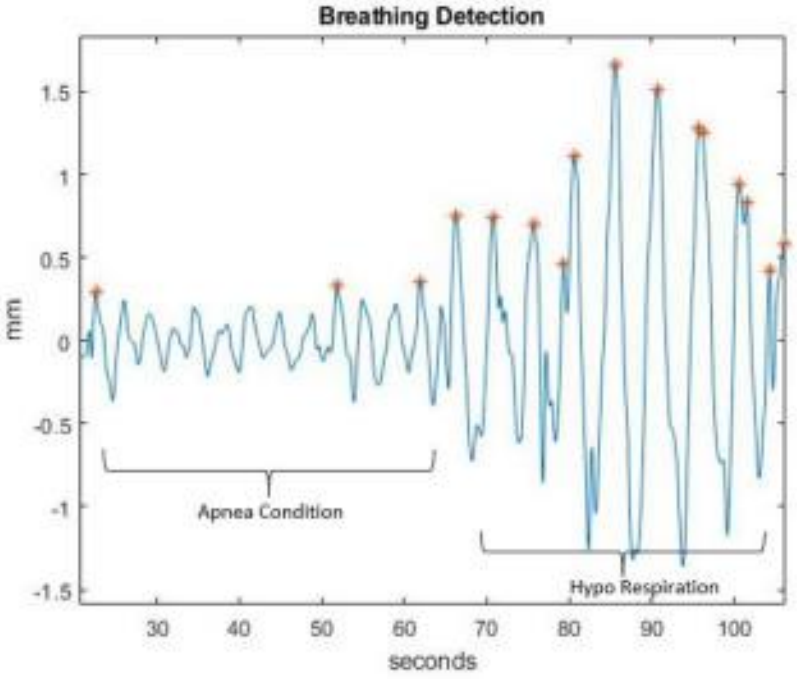

Figure 14: Apnea Condition followed by hypo breathing event.

4- Electromagnetic sensor

- **System design**

Since biological tissue such as skin, particularly lung, has certain conductivity characteristics, its movement can be monitored by using electromagnetic methods. Respiration pattern is then obtained from the inferred proximity timing read by the sensor coil.

Hardware design comprises magnetic sensor and phantom (with pumping mechanism). Air circulation from oxygen tank is regulated by electronics-controlled solenoid valve. It manages human normal respiration pattern and air volume in the lung phantom. Meanwhile, magnetic sensor will detect phantom's conductive surface and provide inductance value in accordance with proximity between the two [38]. Those measured results are then acquired as raw data to be monitored and analyzed. In addition, there is graphical user interface (GUI) which comes with LDC1000 module as reference assessment. The instrument design is shown in Figure 15.

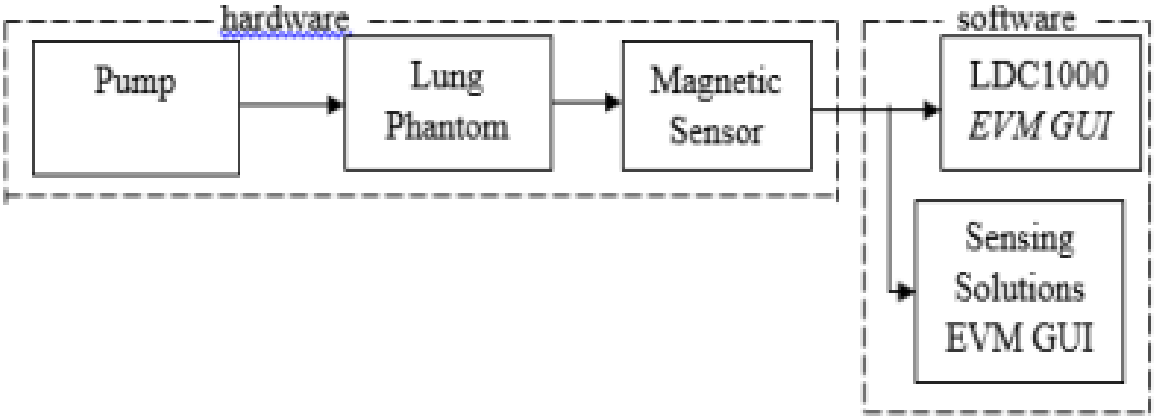

Figure 15: Respiration monitoring system block diagram

Lung phantom is fabricated resembling the real human lung (male) according to reference of pervious research with CT (Computed Tomography) images [38]. Table 3 shows detailed dimension.

	Lung	Male	Female	Combined
Peak to peak		8.9 ±1.1 (8.9) cm	7.7 ±0.9 (7.6) cm	8.3 ±1.2 (8.2) cm
Height	Left	21 ±2.1 (21.8) cm	19 ±2.5 (20.3) cm	19.8 ±2.6 (20) cm
	Right	21 ±2.1 (21.3) cm	19 ±2.5 (19.3) cm	20.6 ±2.6 (21) cm
Max. height	Left	28.2 ±2.2 (27.4) cm	26 ±2.7 (25.6) cm	26.1 ±2.6 (26.5) cm
	Right	21 ±2.1 (21.3) cm	26 ±2.7 (26.3) cm	26.9 ±2.7 (26.9) cm
Width	Left	12.3 ±1.1 (10.6) cm	11.1 ±1 (9.7) cm	10 ±1 (10) cm
	Right	12.3 ±1.1 (12.3) cm	11.1 ±1 (11.2) cm	11.6 ±1.2 (11.4) cm
Depth	Left	18 ±1.5 (18.4) cm	16.2 ±1.7 (16.2) cm	17.1 ±2 (17.1) cm
	Right	18 ±1.5 (17.6) cm	16.2 ±1.7 (15.9) cm	16.9 ±1.8 (17) cm
Volume	Left	2738 ±533 (2817) cm^3	1968 ±505 (2028) cm^3	2301 ±636 (2262) cm^3
	Right	3121 ±605 (3226) cm^3	2300 ±547 (2332) cm^3	2663 ±667 (2583) cm^3

Table 6: Lung Size by CT Images

The phantom is made of silicon material, fiberglass, color pigment, and plastic mold. Elasticity of silicon is good for lung phantom to inflate and deflate. As this research needs conductive surface to impose inductance, additional thin copper sheet envelope is also assembled. Figure 3 shows lung phantom design along with its physical laboratory prototype [38].

Figure 16: Lung phantom design and prototype

- **Monitoring analysis**

Experiment was set involving oxygen tube (air supply), solenoid valve (controlled gate), relay, Arduino Uno (controller electronics), and lung phantom (as shown in Figure 17). Programming on microcontroller was composed for setting solenoid valve channelling oxygen tube and lung phantom. Initially, both of solenoid valves are closed for 3 seconds [38]. Then, solenoid valve on oxygen tube will open for 2 seconds, while on lung phantom is still closed. After 2 seconds, solenoid valve on oxygen tube will close for 2 seconds and on lung phantom is opened. Then, both of solenoid valves will close again for 1 second. These operations are maintained during experiment.

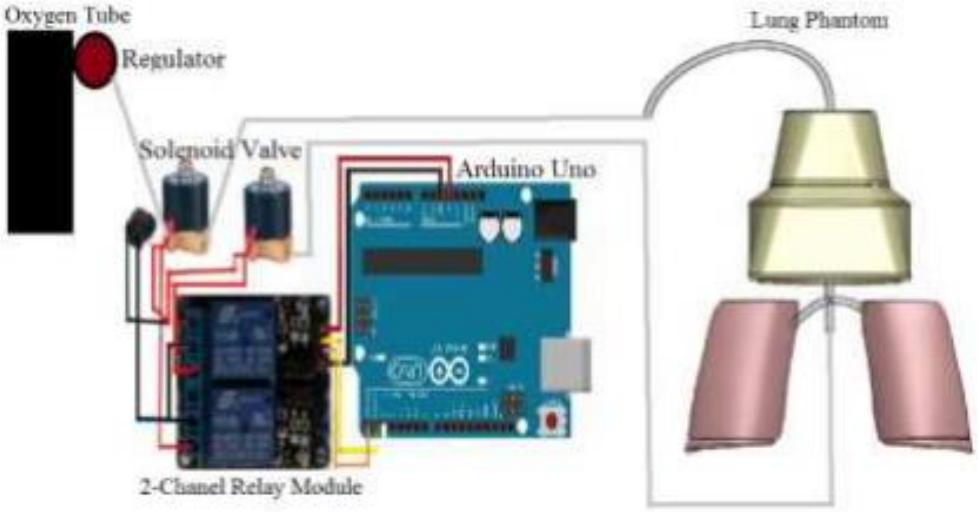

Figure 17: Hardware assembly

Monitoring system incorporates magnetic sensor LDC1000 connected into laptop port. Lung phantom can inflate and deflate automatically like human's respiration pattern. Magnetic sensor will read inductance value and proximity of lung phantom. The result will be shown on LDC1000 EVM GUI. Figure 18 shows the setup of monitoring system.

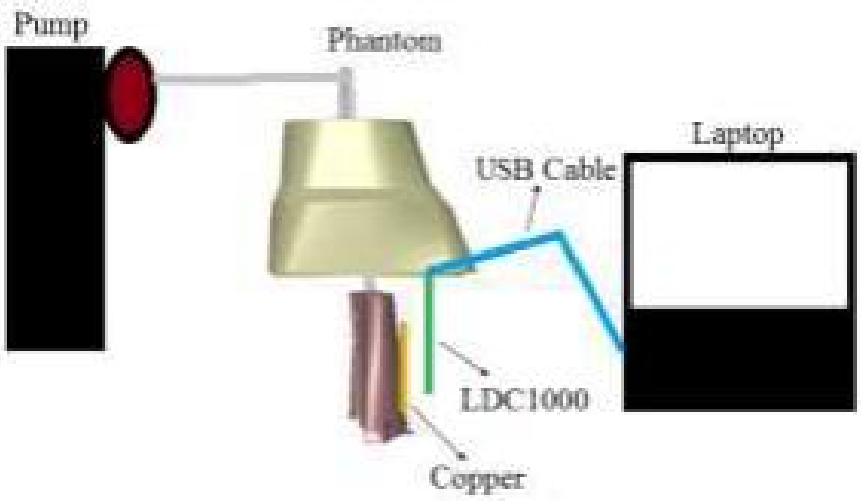

Figure 18: Monitoring system setup

- **Results**

Normal respiration static data which contains inspiration and expiration (with stop) was compiled to produce inductance graph in Figure 19. Note that horizontal axis (distance in mm) is arranged reverse mirrored so that the pattern can be obviously seen. For continuous monitoring in real-time operation, LDC1000 EVM GUI was used providing proximity and inductance data as captured in Figure 20 [38].

Figure 19: Lung Phantom static data of normal respiration

Figure 20: Continuous proximity and inductance monitoring via GUI

The LDC1000 is a sensitive sensor; hence small distance change will affect the result. Air flow was also set to the time of real lung when inflate and deflate, i.e.: two seconds for inspiration and expiration, whereas one second for stop. Comparison between static (manual) and continuous real-time (auto) inductance values at respiration stages is described in Table 4.

Stage	Continuous (uH)	Static (uH)
Inspiration	8	7.805094
Expiration	17	16.469637
Stop	17	16.469637

Table 7: Comparison Continuous vs Static Experiment

There is difference of inductance level between continuous and static experiment. In continuous auto mode, the volume of air supplied into lung phantom is different from the volume of air involved in the real human respiration. This is due to simplicity for demonstrating inflate and deflate of lung phantom. For static manual mode, the volume of air supplied into lung phantom is similar like the volume of air in the real human respiration.

5- Radar

- **Theorical model**

During respiration, the chest volume is changed due to muscle contraction and relaxation. As a result, a pressure difference is generated between the internal and external environments of the chest. Air flows from the high-pressure area to the low-pressure area, periodically entering and exiting the lungs. The motion of the thorax and abdomen is driven by respiratory motion. The body shape is changed as a result of abdominal motion. Consequently, the RCS is changed, and

thus, the amplitude of the received signal changes. In this way, the human respiratory state is detected. A radar system based on this biological mechanism, forward scatter radar (FSR) which is sensitive to RCS changes is introduced. As a special bistatic radar system, FSR is characterized by a bistatic angle reaching up to 180° [39]. Existing studies mainly focus on FSR detection of objects such as stealth aircraft, unmanned aerial vehicle (UAV), and automobiles [39]. FSR has a very interesting feature: With a bistatic angle of less than 180°, the change of RCS only depends on the projection outline area of an electrical conductor and the wavelengths of electromagnetic wave signals; the surface wave absorption features of the target are irrelevant (it is insensitive to clothing textures during human respiration detection). To the best of our knowledge, respiration detection with FSR has not been well investigated in existing literature. The main idea of most existing studies is to detect the micro-Doppler features changed by chest wall micromotion. In this paper, we found that the amplitude of the received signal changes with the changes as a result of human respiration. Figure 21 shows the RCS change pattern of the FSR radar [39].

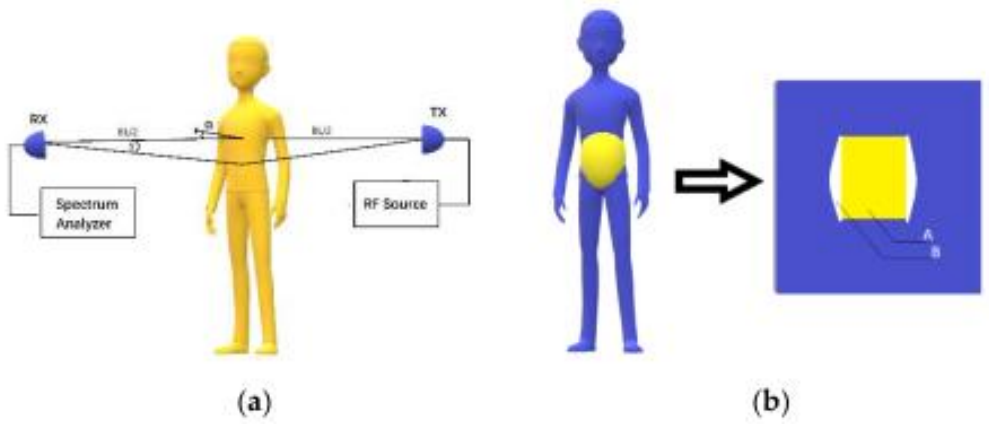

Figure 21: (a) Forward scatter radar structure; (b) changes in the frontal projection of the human abdomen during breathing

As shown in Figure 21a, BL is the baseline, namely, the connecting line between the transmitterand the receiver. α is the included angle between the normally oriented human and the baseline; it isdefined as the orientation angle. δ is the antenna beam angle.

As seen in Figure 1a, the thorax expands and the abdomen gets larger during human inhalation, so Radar Cross Section (RCS) increases. During exhalation, the external intercostal muscles and diaphragm muscles relax, and the abdomen gets smaller, so RCS decreases. As seen in Figure 21b, RCS values can be estimated with the Babinet method.

- **Experimental setup**

In this experiment, a PVDF (polyvinylidene fluoride) piezoelectric film sensor (IPS-17020, manufactured by ZHIMK company in Shenzhen, China) was used. The respiratory rate could be accurately detected with the contact detection system. Meanwhile, a universal WIFI directional antenna with a lower cost was used instead of a copper sheet antenna. Figure 22

shows the diagram of the experiment. In Figure 22a, A is the transmitter antenna, B is the receiver antenna, and C is the PVDF sensor, which was positioned around the chest. The horizontal wave lobe was 105°, and the vertical wave lobe was 70°. As seen in the experiment shown in Figure 22a, the distance between the transmitter and the receiver was 76 cm. The subject turned his back to the transmitter, while sitting in the midpoint between the transmitter and receiver. The distance between the subject's back and the transmitter was 20 cm. The height of the antennas and of the navel was 65 cm [39].

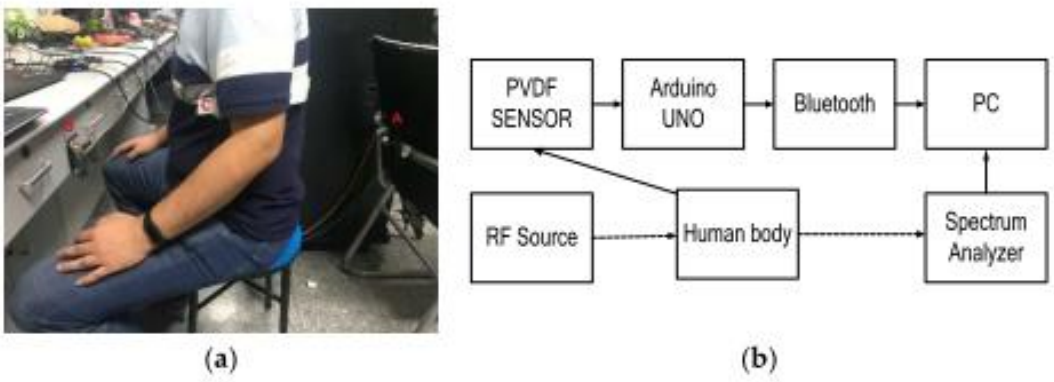

Figure 22: (a) Experiment setup in the common room; (b) the experiment system block diagram

The whole experimental process is displayed in Figure 23. First, the radar emitted a 2.4 GHz continuous wave signal. When the radio wave had a diffraction around the abdomen, the change in belly size modulated the carrier in amplitude. Second, at the radar receiver, the breath curve was acquired through envelope detection. Finally, the respiration rate could be perceived after peak detection. The respiration detection results of FSR were measured at orientation angles α of 0, 30, 60, and 90°, respectively.

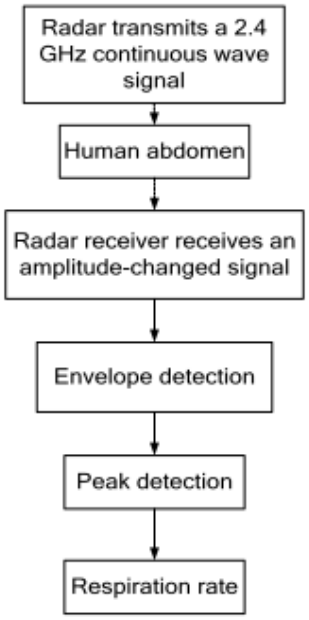

Figure 23: The flowchart of the proposed FSR system.

- **Results**

The experiment results are shown in Figure 24.

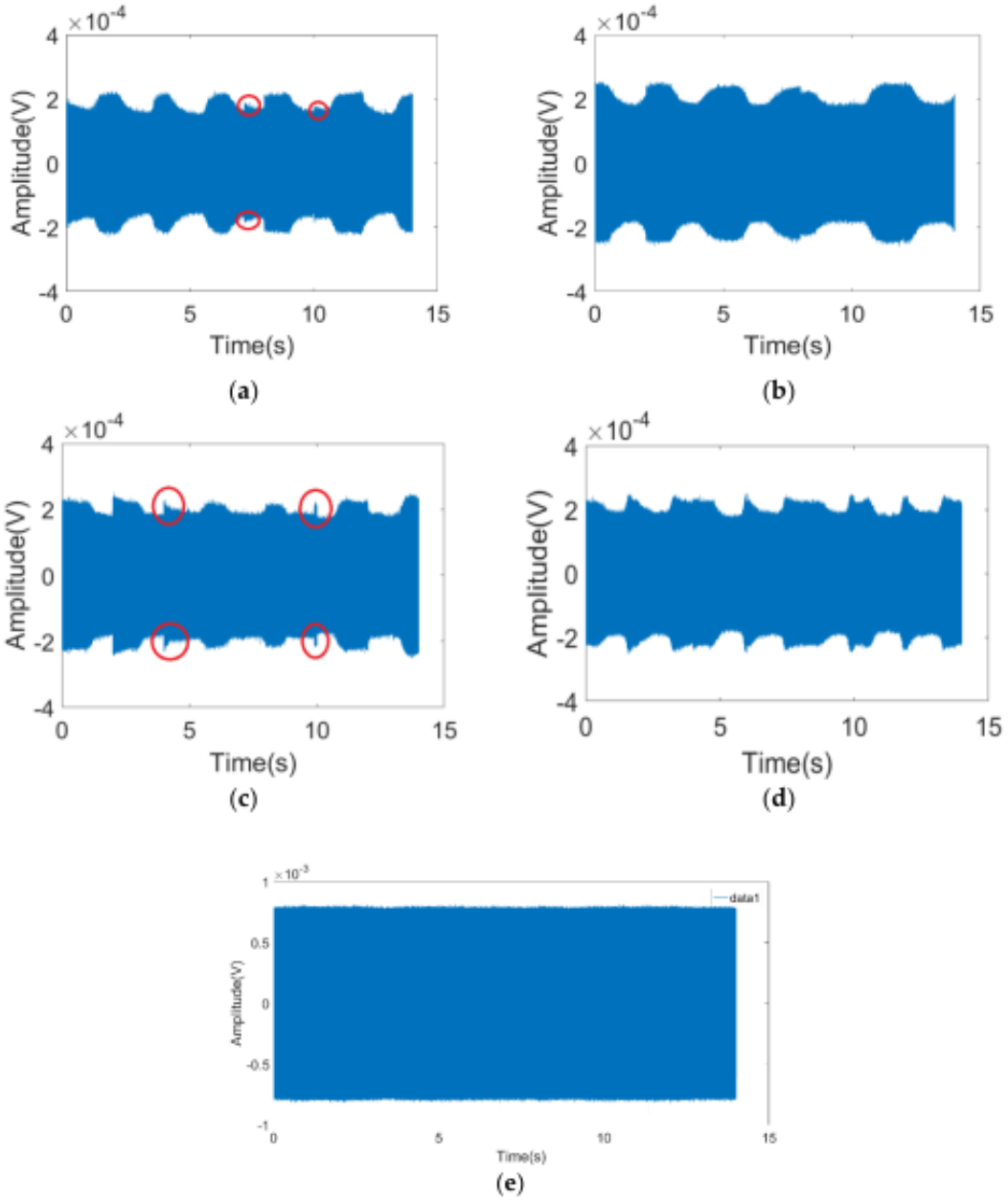

Figure 24: The received signal of the FSR system with a different orientation angle α for (a) 0°; (b) 30°; (c) 60°; (d) 90°; (e) the received signal of the FSR system with nobody in the test area.

It can be observed in Figure 24 that the detection results of respiration rates were good under the orientation angles of 0, 30, 60, and 90°. In the diagram, peaks marked with round circles were generated from random physical motion. It was found that human motion was very short in the timeline in comparison with respiration; it could be easily distinguished from respiration through observation within a continuous time threshold. The output of the envelope detection is shown in Figure 25.

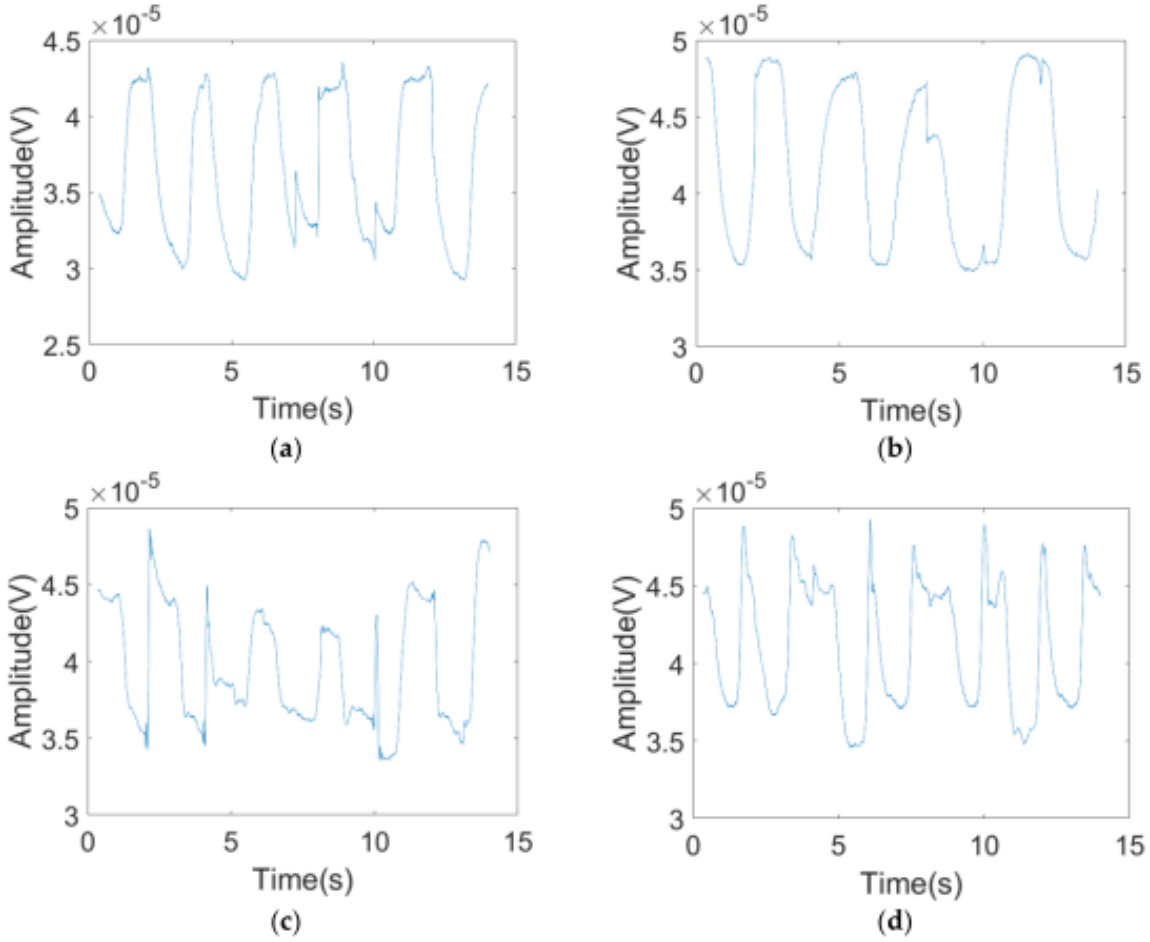

Figure 25: The output of the envelope detection with the different orientation angle α for (a) 0°; (b) 30°; (c) 60°; and (d) 90°.

Finally, to demonstrate the effectiveness of the proposed FSR system, we compared PVDF with FSR signals in the cases where the angle was 0 or 90°. We executed the experiment with the same setup used in the second experiment. The results of multiplying the FSR signal with a scaling factor are shown in Figure 26. In Figure 26a, it can be observed that the FSR signal fits well with the PVDF signal when the angle is 0◦; the respiration rate is 22.5 times per minute [39]. The respiration rate obtained from the PVDF signal is the same as that from the FSR signal. In Figure 26b, when the angle is 90°, the two curves are slightly different due to the fact that the waveform of the FSR changes more violently when the orientation angle is 90°. RCS is influenced by the changing of orientation angles. There was more fat on the front face of abdomen, so skin micromotion was more violent during its expansion and contraction. In Figure 26b, although there are mismatches between the PVDF signal and the FSR signal, both the PVDF signal and the FSR signal show the same respiration rate. At the angle of 90◦, the respiration rate is 19.2 times per minute [39].

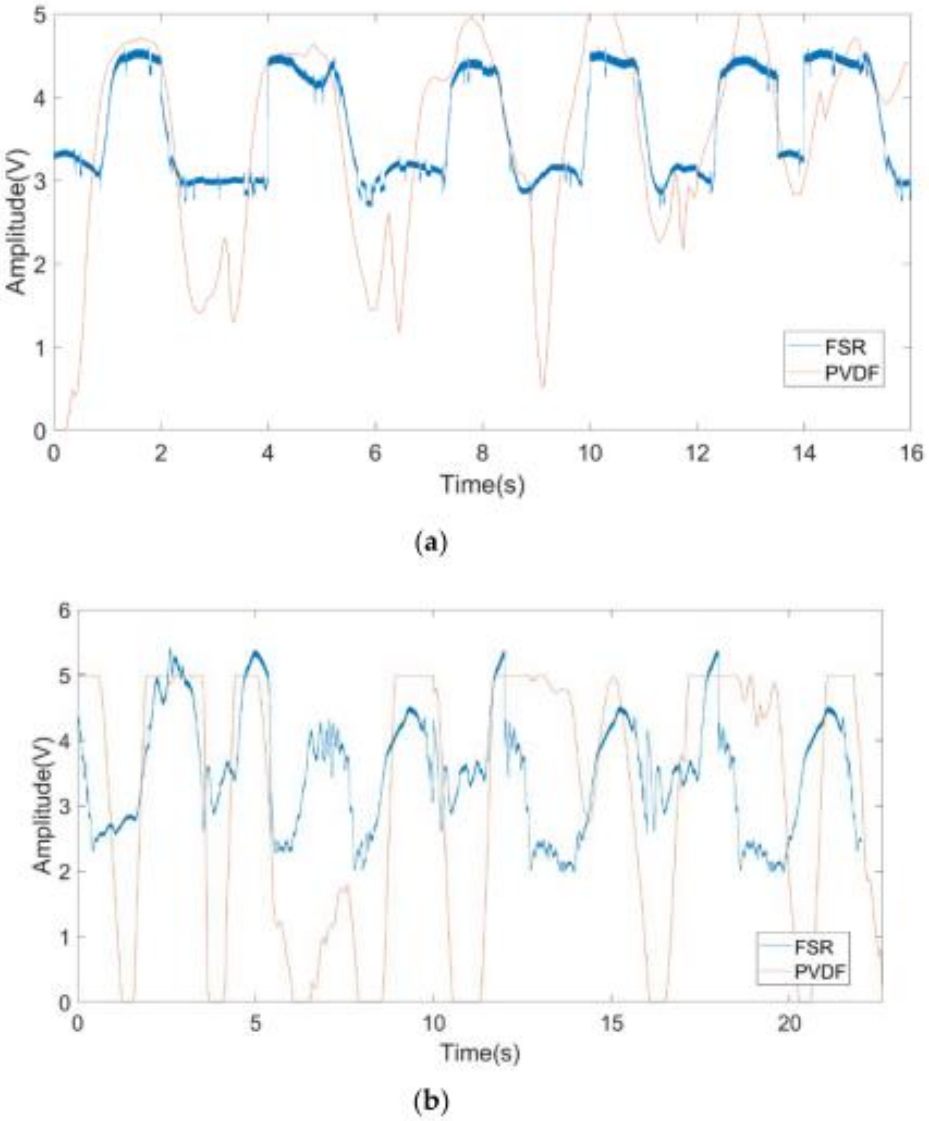

Figure 26: The comparison between FSR and PVDF (polyvinylidene fluoride) with the different orientation angle α for (a) 0°; (b) 90°.

Finally, It was found that the system had a high robustness with respect to the subject's clothing. The first experiment was made in winter. The subject wore two layers of clothes. The first layer was made of chemical fibers and the second layer was made of cotton. The second experiment was made in summer, and the subject wore one layer of clothes made of cotton. Obviously, despite the texture, thickness, and number of layers of clothes, the system's detection results were good due to the characteristics of FSR.

III- METHOD FOR CARDIAC RATE

1- IR-UWB

- **Measurement system and experimental setup**

Participants stayed at rest for 5 minutes until they reached a comfortable condition before the data acquisition using the IR-UWB radar [18]. When a comfortable condition was not achieved after 5 minutes, participants took an additional 5-minute rest before the measurement. The data were acquired in the supine position with clothes on. Heart beats were simultaneously measured from the IR-UWB radar and ECG so that the data recorded from the two devices were synchronized. Participants were told to hold their breath for 15–20 seconds during the measurements, to minimize the noises from the chest wall during respiration [9].

The detailed settings for the radar measurement are depicted in figure 27A. A commercially available IR-UWB radar device, X4M06 (Novelda, Oslo, Norway) was used to send and collect the radar signals to and from the heart [18] . The radar device has been certified by both Korea Communications Commission and Federal Communications Commission. The radiation power of the radar device was 68.85 μW, and in the central frequency of 8.7 GHz, the penetration depths where the power decreases to 1/e of the original power was estimated to 1.6 mm for skin and 1.4 mm for muscles. The detailed processes of the data acquisition are described in figure 27B. For acquiring, processing and storing the data from ECG and the radar, MATLAB was used. A single bipolar lead ECG was measured simultaneously with the radar using an ECG device, PSL-iECG2 (PhyioLab, Pusan, Republic of Korea). The electrodes for the ECG device were placed on both wrists and the left elbow joint, and the data from the limb lead II were obtained [9].

IR-UWB radar devices transmit signals and receive them when they are reflected by obstacles. In a radar system, the received analog signals are sampled and quantized by an analog-to-digital converter (ADC) to become digital data. The digital data were transferred to MATLAB for further data processing. Because the received signals contained various noises outside the frequency range, we canceled the noises using the bandpass filter. These raw radar signals contained various unwanted background noises within the radar bandwidth, called clutter signals, along with the target signals for heart movements figure 27C [9].

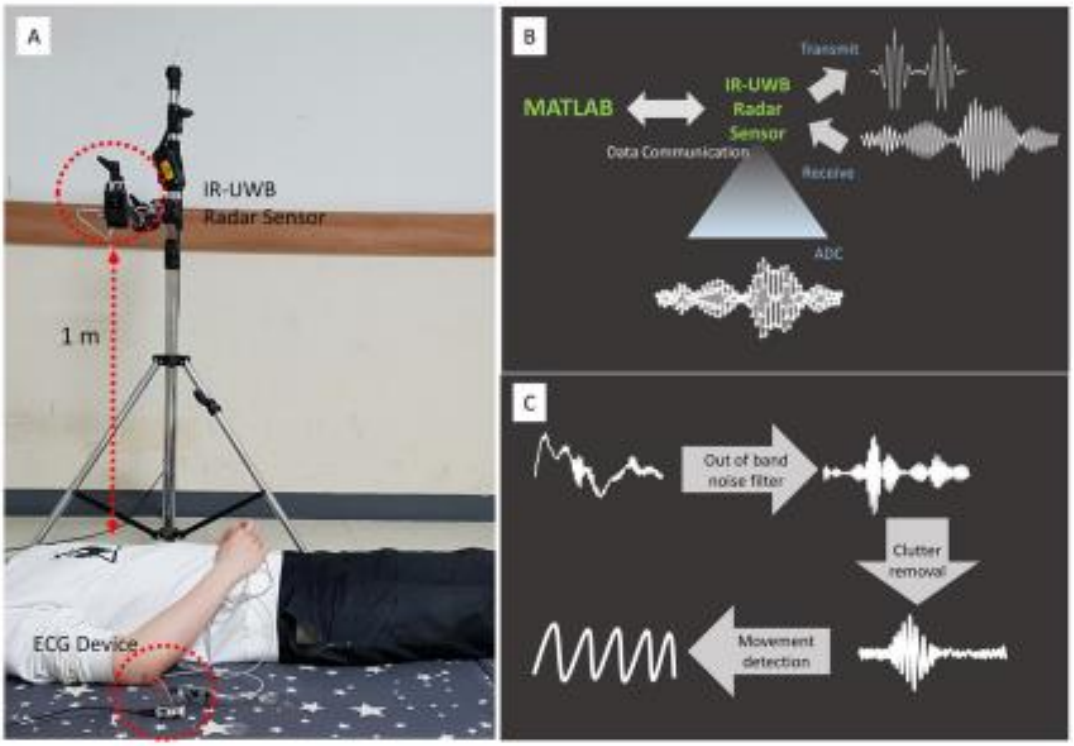

Figure 27: Acquisition and processing of the IR-UWB radar signals from the heart. (A) The experiment was conducted with participants whose clothes were on after 5–10 minutes' rest. (B) The IR-UWB radar system transmitted radiofrequency pulse waves and received signals reflected from an object. (C) The raw signals passed through a bandpass filter to cancel noise, then were processed to separate clutter signals from target signals.

- **Results**

The waveforms obtained from IR-UWB radar and ECG in healthy volunteers and patients with AF are shown in Figures 28A and 28B. In the healthy volunteers with normal sinus rhythm, we found that HR, average R-R interval and individual R-R interval measured in the radar showed high agreements with those measured in ECG. The average R-R interval showed the highest agreement level, while the individual R-R interval showed lowest agreement level between the 2 measurements. The 95% confidence intervals (CIs) of the mean biases included the lines of equality in all 3 parameters, indicating no significant biases between the ECG and radar parameters [9].

In the patients with AF or other diseases, HR and average R-R interval measured in the radar also highly agreed with those measured in ECG, and the same was observed in healthy volunteers, whereas individual R-R interval showed a slightly lower agreement level. Using the 3 criteria of AF, we automatically determined the presence or absence of AF in healthy volunteers and patients with AF.

Non-invasive heart monitoring modalities, including ECG and pulse oximetry, are widely used in daily clinical practice. However, to date, there is no established modality to monitor heart beats without physical contact. Non-contact heart monitors would have many advantages over conventional heart monitors, which limit the patient's mobility, cause local problems associated

with electrode attachment such as skin eruptions, abrasion and bruise, transmit contagious diseases and require occasional replacement if the device will be in prolonged uses.

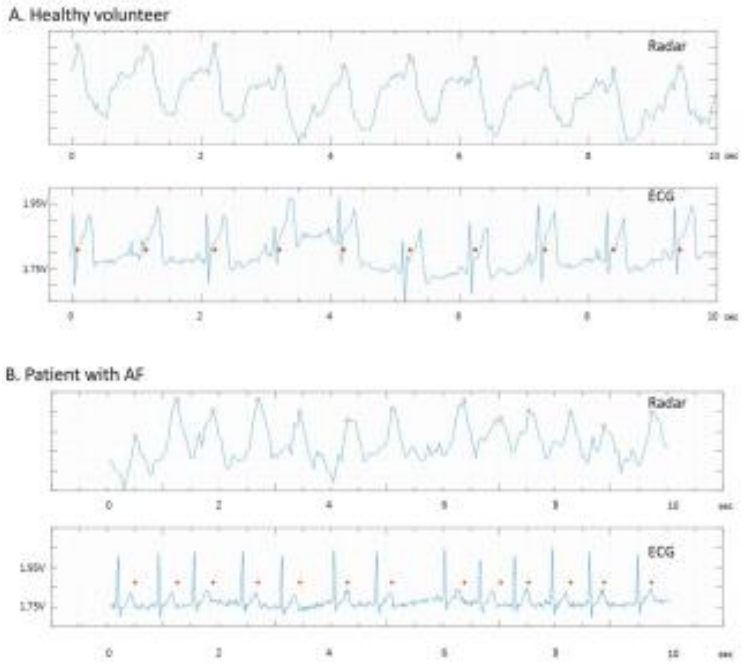

Figure 28: Examples of the heart signal waveforms obtained from the IR-UWB radar. The agreements between the radar and ECG were grossly excellent in both the healthy volunteers with NSR (A) and the patients with AF (B). The red dots indicate the same time points on both the radar waveform and ECG.

2- Microwave sensor

- **Experimental system**

In Figure 29, the microwave Doppler sensor outputs Doppler waves I(t) and Q(t) by mixing a transmission wave TS(t) and a received wave RS(t). In this work, we employ a 24-GHz microwave sensor; only I(t) is used to detect the heart beat [10]. The most important problem of the microwave Doppler sensor for heart rate monitoring is human body motion artifacts and to eliminate the body motion artifact, we introduce a sensor fusion approach, which uses both a microwave Doppler sensor and range imagery as presented in Figure 29. The range imagery obtained by Microsoft Kinect is used to estimate the body motion velocity using the change of the distance from the body surface. It has 5 mm resolution at 30-cm distance by averaging 121 pixels.

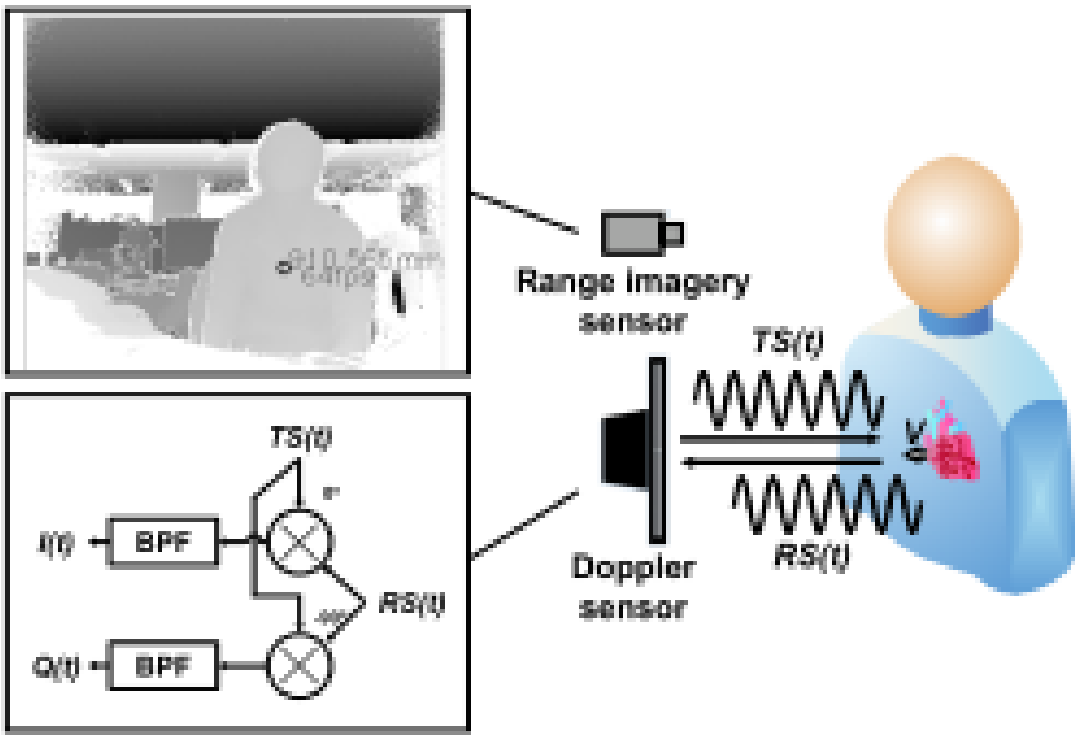

Figure 29: Heart rate monitoring system using microwave Doppler sensor and range imagery.

- **Measurement setup**

To evaluate the proposed system and algorithm, we measured the Doppler wave, range imagery, and the heart rates for some subjects. The measurement duration was 60 s. Figure 30 presents the experimental setup. The subjects were measured in a sitting posture because we assumed an in-vehicle system application. All subjects were measured at rest and with body motion conditions.

Distance between the subject and the range imagery sensor (Microsoft Kinect for Windows v2; Microsoft Corp.) was set to 80 cm. The microwave Doppler sensor (NJR4232K1; New Japan Radio Co. Ltd.) was also set to 30-cm distance from the subject [10]. An accurate heart rate was recorded simultaneously using an adhesive patch type ECG sensor (Actiwave Cardio; CamNtech) for use as a reference for performance evaluation. The required computational time to extract heart rates from the Doppler sensor output with 30 s duration is 6.32 s on average [11].

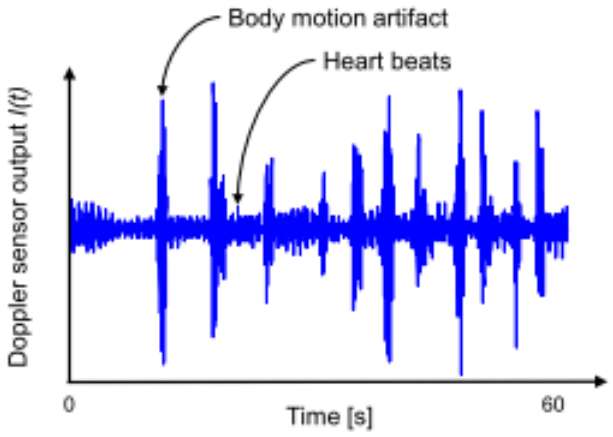

Figure 30: Doppler sensor output with body motion artifact

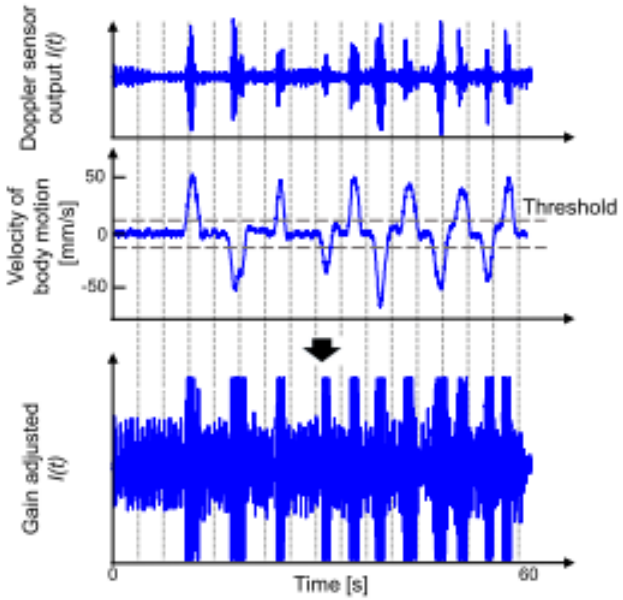

Figure 31: Gain adjustment of Doppler signal with body motion artifact.

- **Results**

Figure 32 shows measured waveforms and the heart rate extraction result of one subject with the body motion condition. The extracted heart rate was compared with the reference value of ECG sensor and the extracted value using a conventional method, which extracts the heart rate from the time-domain Doppler signal using template matching. Measurement results show body motion artifact suppression. The proposed method correctly extracted the heart rate. The success rate is improved even in a resting condition by virtue of time–frequency domain processing. The success rate with the body motion artifact condition was improved about 75%, on average [11].

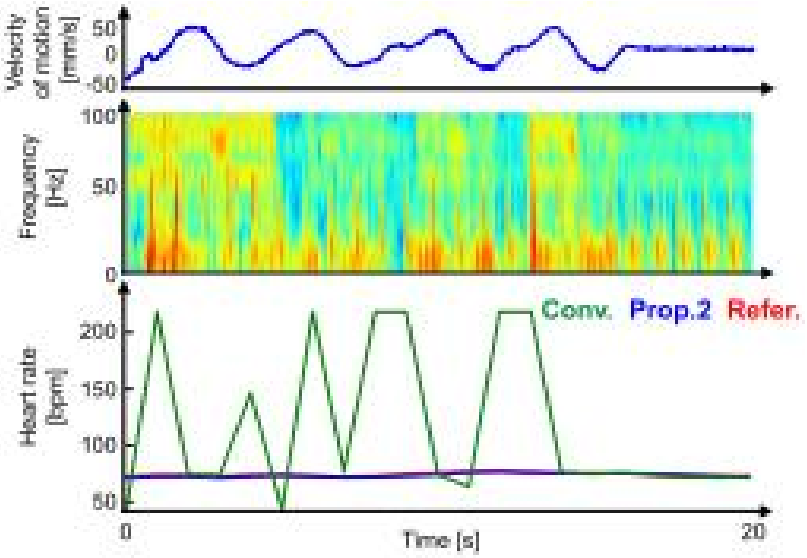

Figure 32: Measurement result of heart rate extraction and comparison with reference sensor and conventional method.

A sensor fusion approach to realize a non-contact and non-invasive heart rate monitoring system using the microwave Doppler sensor and the range imagery was proposed. The proposed method uses time–frequency analysis and body motion artifact reduction according to the velocity information of the body surface, as obtained using range imagery. The measurement results for three subjects in a non-rest condition show that the proposed method achieves 75% heart rate extraction success rate improvement, on average.

3- Ultrasounds

- **Experimental setup**

A commercial Piezo respiratory belt transducer (MLT1132) was applied to the subject's thorax to measure BR for validation purposes. The study adhered to the Declaration of Helsinki ethical principles (Finland 1964). The protocol was approved by local ethics committees (protocol number: 0000034901) [28] . The ultrasonic PING sensor (40 KHz) was placed in front of the subject's thorax at different distances (0.5, 1, 2, and 3 m). The experiment was for approximately 60–120 s for each subject at a room temperature of 15◦C and repeated at different times of the day with different clothing to obtain sufficient signals [28]. One subject was asked to simulate abnormal breathing syndromes by following a defined protocol consisting of 10 s normal breathing, 13 s of high rate breathing, 13 s breath holding, 38 s of low rate breathing, 20 s breath holding, and 18 s of irregular breathing followed by normal breathing. The experimental setup and the annotated photograph of the proposed system are presented in Figure 33.

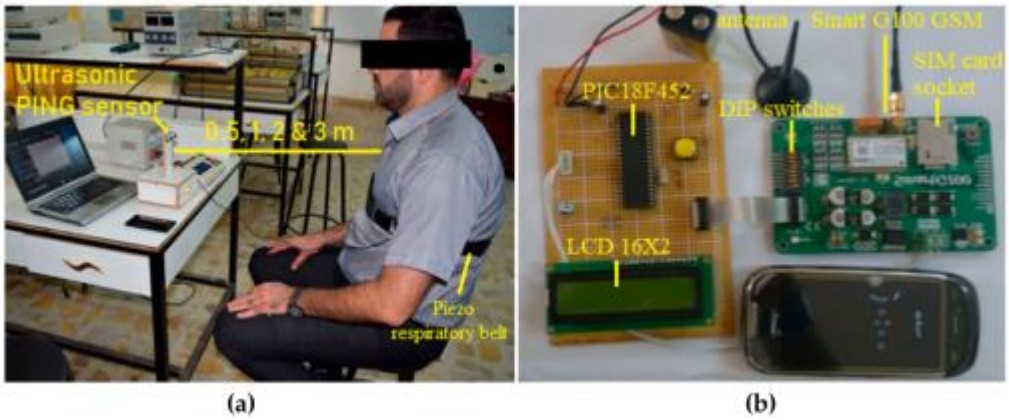

Figure 33: (a) the experimental setup; (b) the annotated photograph of the proposed monitoring system.

- **Measurement setup**

The schematic diagram of the proposed monitoring system is depicted in Figure 34. It can be divided into three main parts: The ultrasonic PING sensor, microcontroller PIC18F452, and smart G100 GSM modem.

The ultrasonic PING sensor is a low-cost range sensor unit developed by Parallax Inc. (Rocklin,CA, USA) [29] . This sensor detects the reflection, or echo signal from an obstacle (subject's thorax) and evaluates the propagation delay and amplitude of the return signal. This sensor provides accurate and remote distance measurements from 2 cm to 3 m with spatial resolution of 0.3 mm [29] . The sensor was connected to a PIC18F452 microcontroller, which was programmed to send a pulse, then to start an internal timer (16 bits) to measure the time interval in µs before the echoes were received. The echo pulses were then used by the PIC18F452 to calculate the difference in thorax displacement. The ultrasound-based distance detection principle was used to accurately detect thorax displacement.

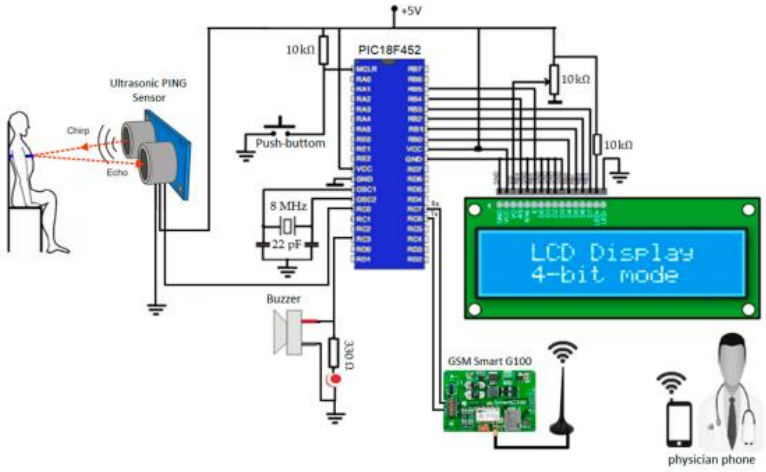

Figure 34: Schematic diagram of the proposed monitoring system.

- **Results**

One healthy subject (37 years) performs a defined protocol simulating normal and abnormal breathing syndromes for a period of two minutes [30]. The subject was seated in front of the ultrasonic PING sensor at approximately 1 m and he was first asked to breathe normally for 10 s and then breathe quickly for 13 s and hold his breath for 13 s followed by slow breathing for 38 s and hold his breath again for 20 s followed by irregular breathing for 18 s and back to normal breathing [29]. The breathing signal was recorded using PowerLab data acquisition software provided with Piezo respiratory belt transducer (MLT1132; ADInstruments Pty Ltd., Australia) at a sampling rate of 1000 Hz and compared with the breathing signal obtained by the proposed monitoring system as shown in figure 35.

Figure 35 proposed monitoring system could successfully and effectively detect the normal and abnormal breathing events, including eupnea, tachypnea, bradypnea, central apnea, and irregular breathing and could send an alarm message when the breathing signal fell outside the normal range or when breathing stopped or became irregular.

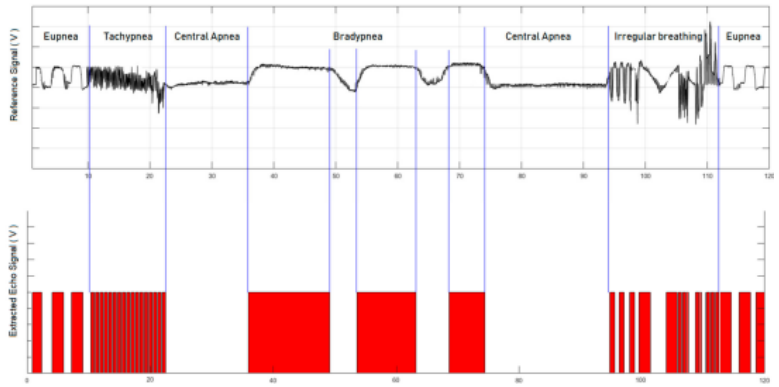

Figure 35: The breathing signal obtained by the reference system (upper trace) and the breathing signal obtained by the proposed monitoring system (lower trace).

In this study, they have developed a real-time, non-contact, non-invasive, low cost, low power consumption, portable, and precise monitoring system for detecting the normal and abnormal breathing activity at a distance of up to 3 m for fully clothed subjects using the ultrasonic PING sensor, PIC18F452 microcontroller, and smart G100 GSM modem. Continuous monitoring of breathing activity could facilitate a more thorough and adequate assessment for early recognition of abnormal breathing syndromes.

4- Infrared/RGB camera

- **Measurement system**

The blood vessels throughout the body are broadly categorized as arteries or veins, and there is a difference in the way the volume of blood flowing through each blood vessel type changes. Blood flow volume through veins changes little, whereas blood flow volume through arteries

varies according to the pulse. Further, one of the properties of oxygenated haemoglobin in the blood flowing through arteries is that it easily absorbs light from a specific wavelength. Because of these properties, when the skin is exposed to continuous light of a specific wavelength, the reflected light changes according to variation in blood flow volume, and the pulse waveform can be obtained by continuing to measure that reflected light [23] .

Figure 36 shows the principles of measuring heart rate using infrared/RGB facial-image analysis. The simplicity and non-invasiveness of obtaining measurements with a photoplethysmography (PPG) sensor have led to the PPG sensor's application as a tool for monitoring health [24, 25]. In PPG sensors, light is emitted from a dedicated light source (wavelengths 660 and 940 nm), and the volume pulse wave is obtained by measuring the reflected light with photodiodes. In this study, heartbeat was measured with an RGB camera by substituting ambient light for the dedicated light source and an RGB camera for the photodiodes and then measuring the form of the volume pulse wave in the same way as in PPG. Because of the degree of skin exposure and ease of detection, the heartbeat waveform was measured from the face.

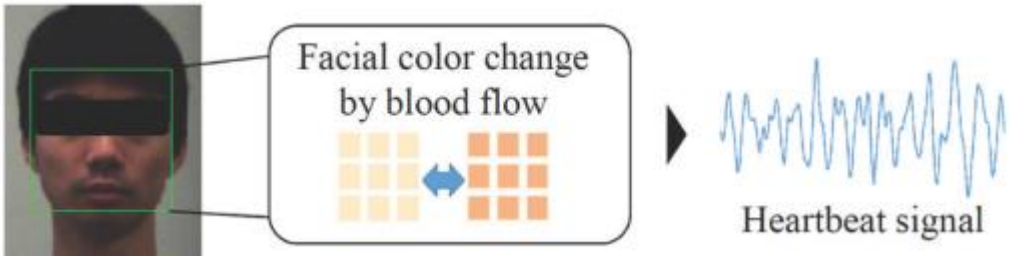

Figure 36: Principles of measuring heart rate using infrared/RGB facial-image analysis.

- **Experimental setup**

The experiment was conducted with ten healthy university students. An infrared/RGB camera was set up 50 cm in front of the measurement subjects, and the subjects were instructed to sit and maintain a resting state. Images were taken for 30-s periods when at rest and after exercise (ergometer exercise: 70 rpm, 100 W, 2-min duration) [23]. Furthermore, measurements were also taken simultaneously using thoracoabdominal respiration sensors and an electrocardiogram as references for respiratory rate and heart rate, respectively figure 37.

A band-pass filter (0.17–0.42 Hz) was applied to this waveform by a signal processer. Then, the waveform was normalized, and the autocorrelation function was calculated. Meanwhile, the visible images taken with the RGB camera were converted to a single color (green), and an area centered on the nose (150 × 180 pixels) was extracted. The luminance values calculated were recorded over time to create a waveform. A band-pass filter (0.83–2.5 Hz) was applied to this waveform. Afterward, the same type of processing as in respiratory rate calculation was performed to calculate the heartbeat.

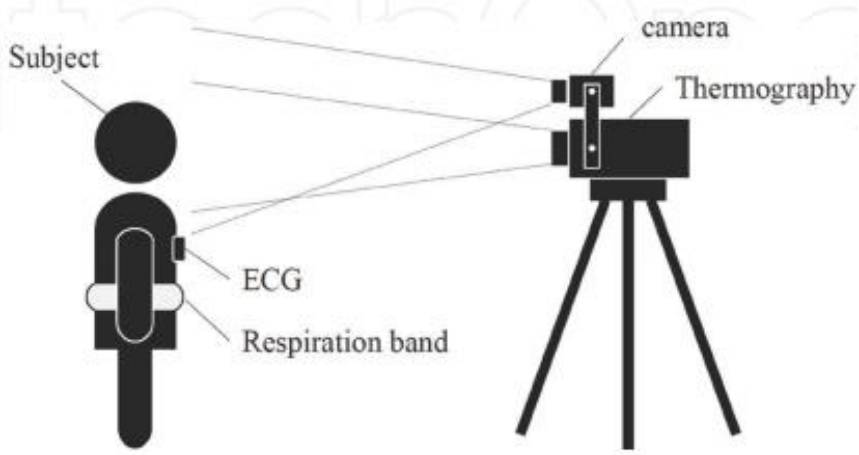

Figure 37: Experimental protocol.

- **Results**

Figure 38 shows the heartbeat curves obtained from the ECG and visible images. They demonstrate that heartbeat is like the curves obtained from the references. The results for heart rate were as follows: a correlation coefficient of 0.96 ($p < 0.01$), an average difference of − 0.27 (beats per minute) between the respiratory rates obtained from the visible images and ECG, and a 95% confidence interval of − 6.1 to 5.5 (beats per minute). These results demonstrate that highly accurate measurement of respiratory rate and heart rate are possible, regardless of how those values fluctuate (respiratory rate: 9.2–23.9 breaths per minute, heart rate: 47.9–93.9 beats per minute) [23].

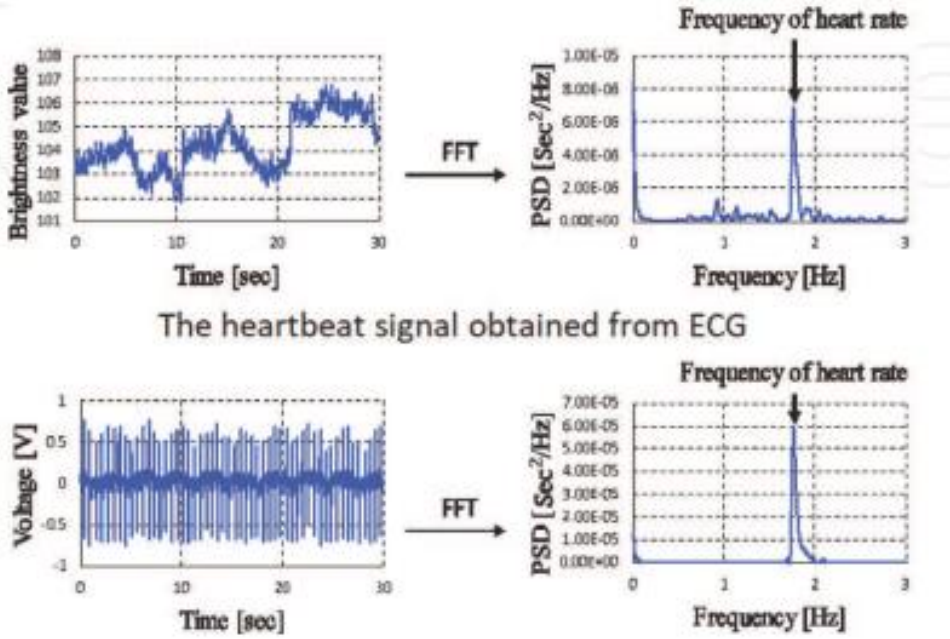

Figure 38: Heartbeat curves obtained from ECG and visible images. The heartbeat signal obtained from RGB camera.

Looking toward future practical applications, elimination of noise caused by body movement and a face/nose tracking function for automatic measurement of heart and respiratory rates will likely be added, improving the accuracy and stability of measurements, and we can expect this technology to be applied in a variety of ways.

5- Laser

- **Experimental setup**

A diagram of the experimental arrangement used to monitor the heartbeat is shown in figure 1. It comprises a low-power laser, the organism, a fibre optic bundle, a photodiode and a data acquisition–monitoring system [40]. The light illuminates the moving organ and some of it is reflected. This reflected light is collected with the fibre optic bundle and sent to a photodiode connected to the data acquisition system.

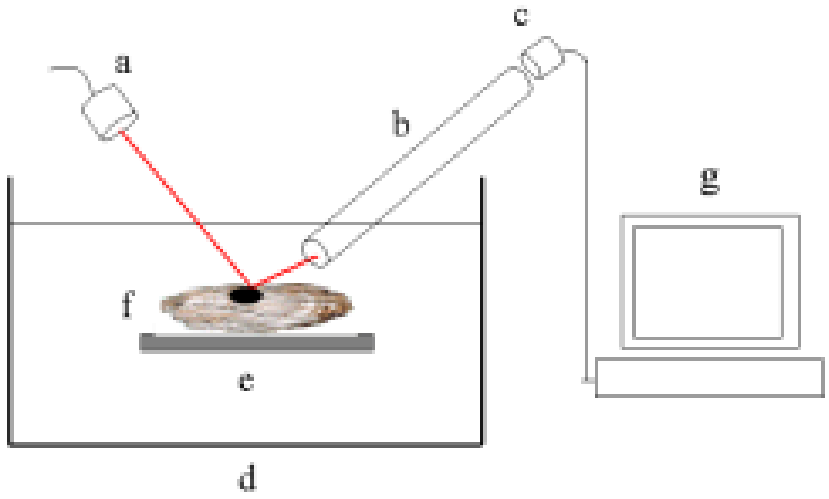

Figure 39: Schematic representation of the experimental set-up used to monitor the beating of the heart: (a) red low-power laser diode, (b) fibre optic bundle, (c) germanium photodiode, (d) water receptacle, (e) hydraulic device to position the mollusc, (f) the oyster and (g) the data acquisition–monitoring system.

The laser beam is sent onto the moving sample, and the reflected light is captured by the fibre optic bundle that sends the light into the germanium detector. Finally, the electrical signal is sent to the data acquisition–monitoring system.

The general idea of the method is to relate the change in time of the voltage recorded by the photodiode with the variation in the intensity of the reflected light captured by the bundle, and then to relate the intensity of the reflected light to the movement of the sample under study. The intensity of the light collected with the fibre optic bundle can vary for two reasons. One is the geometric acceptance of the system. When the organ moves it may reflect the light to a place outside the acceptance of the detector. The second reason is a variation in the intensity of the reflected light itself, due to changes in the reflectance of the organ while moving. In order to be able to concentrate on the second effect we have developed a simple model to account for the different possible angles of reflection of light from a beating heart, so that a detector system with a given angular aperture can be placed such that it has practically complete acceptance of the reflected light throughout the movement of the sample [43].

- **Measurement setup**

The technical specifications of the components used in the measurements reported here are as follows. A low-power red laser diode of 4 mW and 632 nm was used. The radius of the laser beam was around 1 mm. The fibre optic bundle had a length of 1.3 m and a cross section of 38mm^2. Its transmittance at the chosen wavelength is approximately 60% and its acceptance angle is 82°. A coupled large-area EG&G Judson J16–5SP–R03M–SC germanium photodiode (3×3 mm^2 active size) of high responsivity, good linearity, fast response time, uniform response and excellent long-term stability was selected. In general, the J16 series is designed for operation under ambient conditions up to +60°C [40]. The photodiode voltage signal was acquired with a personal computer, using an AT–MIO 16× data acquisition card connected through a BNC–2080 multiple channel interface board. The system is operated using homemade software based on LabVIEW. The intrinsic time resolution of the system is quite enough for most applications in the study of biodynamics. The slowest component is the data acquisition card, which samples at 200 kHz, but if the case under study requires it, it is possible to use a faster card [40].

Regarding the spatial resolution, one has to take into account on one hand the radius of the laser beam and on the other the absolute size of the intensity variations caused by the part of the organ under study. In principle if only one section of the illuminated sample causes a change in intensity, and the rest of the sample does not, it is possible to detect the variation even when the beam is bigger than the part causing the change. Of course, to isolate a section of an organ it is better to have a small beam. Here we used one with a radius of 1 mm; this was appropriate for the sample under study, but it is possible to change the width of the laser beam using a standard optical arrangement of lenses.

In this experimental set-up the cross section of the bundle is larger than the active area of the photodiode. It has been observed that the combination of the fibre optic bundle plus the germanium detector increases the intensity of the detected light with low additional noise. In a dispersive medium, where bigger detectors are needed, this particular arrangement is very useful because the noise in a photodiode generally increases with the size of its active area. Using optical fibres it is possible to have a bigger acceptance without extra noise.

Finally it is very important to notice that neither electronic nor analytic filters are used in our experimental set-up although they could be added if needed.

- **Results**

Figure 40 shows typical results obtained when monitoring the beating heart of an oyster using the laser reflection technique. Both plots depict the variations with time of the voltage measured by the photodiode. Figure 40(a) displays 60 s of data from an oyster surrounded by air, while figure 40(b) displays 20 s of data from an oyster in salt water. The regular beating of the heart can be observed in both plots as a succession of peaks. Note that these plots were obtained without the use of any kind of analogue or digital filter. The absolute scale of the measured

voltage is arbitrary (it depends, among other things, on the exact location of the detector), but we are only interested in the variations of the voltage.

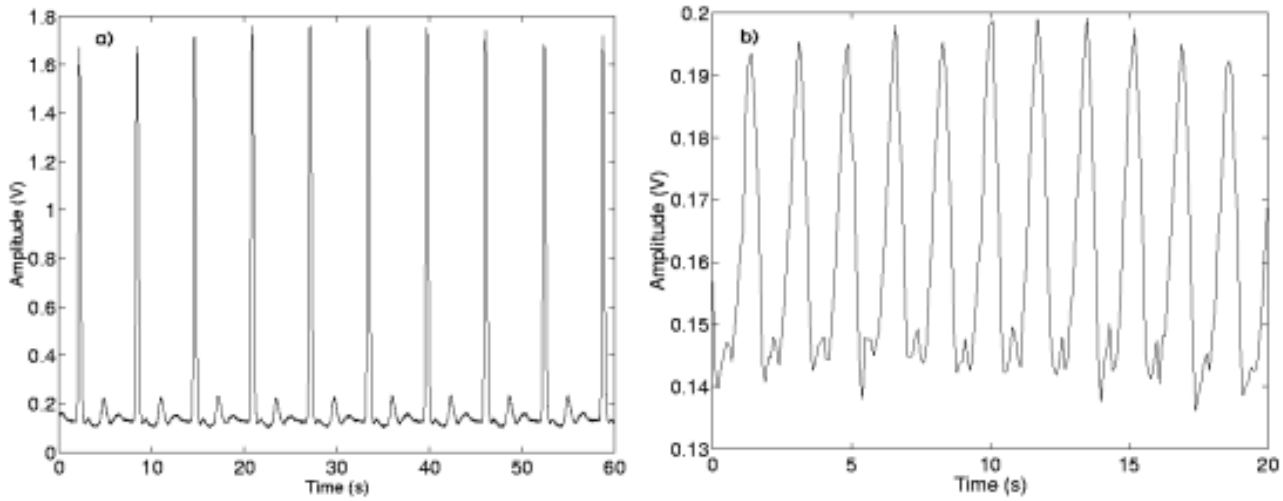

Figure 40: Waveform of the heartbeat of an oyster (a) surrounded by air and (b) in salt water. Depicted is the variation with time of the voltage measured in the photodiode.

The measurements recorded with the organism in an environment resembling its natural habitat, figure 40(b), show more activity. There are 11 heartbeats, one more than in figure 40(a), but in only one-third of the time. Nevertheless, it is still possible to discern clearly both the higher and smaller peaks. The width of the peaks is more or less the same in both plots of figure 40. They look slimmer in the first plot due to the scale and separation between peaks.

The plots of figure 40 show that the method works and even measurements taken for short periods of time allow the extraction of interesting physiological information. When considering longer periods of time other physiological functions come into play and can also be analysed with this technique. In the case of Crassostrea virginica, as well as the cardiac activity, two other contributions to the signal are observed [43].

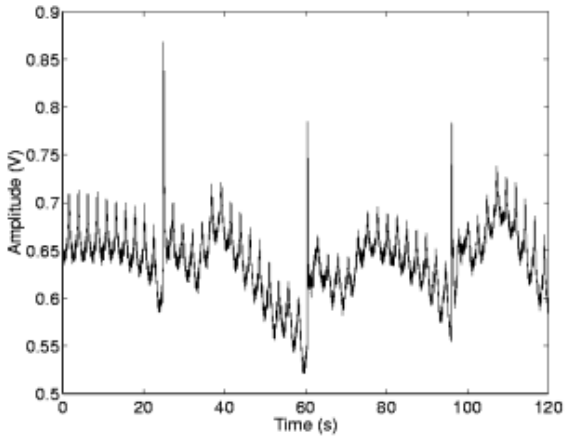

Figure 41: Signal from an oyster immersed in salt water. The signal has three parts. The high frequency fluctuations correspond to the beating of the heart, the modulations with maxima around 40, 80 and 110 s are related to the movement of the gills while the high peaks around 25, 60 and 95 s are identified with the sudden closing of the valves.

Figure 41 shows data for two consecutive minutes from an oyster immersed in salt water, where it is able to perform its basic physiological functions such as respiration and feeding. The heartbeat is seen in the high frequency fluctuations of figure 41, while the slow quasi-periodical modulation with maxima around 40, 80 and 110 s correspond to the activity of the gills. The strong peaks occur when the organism closes its valves rapidly while feeding. Compared with the activity of the gills, this is a less frequent phenomenon. The assignation of these parts of the signal to the physiological functions was made by direct visual observation [40].

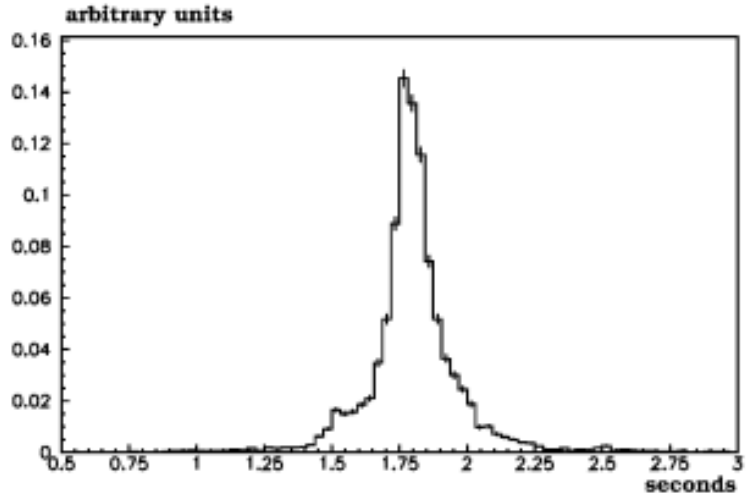

Figure 42: Distribution of the time interval between heartbeats, as obtained from the time difference between two peaks associated with the contraction of the ventricle. The distribution was computed from a 6 h recording.

Recently an analysis of the fluctuations of the interbeat time during long periods of data recording has produced much of interest from the point of view of nonlinear phenomena, as well as a tool for identifying anomalies in the functioning of the heart [41-42]. In order to show that our method could also be used for these kinds of studies we took data series for up to 12 h. Figure 42 shows the distribution of the time interval between heartbeats, as obtained from the time difference between two peaks associated with the contraction of the ventricle. This distribution, corresponding to 6 h of data, shows the typical behaviour of these kinds of systems. Only a few interbeat periods are short, and most of them have a period of about 1.8s; after that a strong decrease in the distribution is observed. Similar results have been obtained previously using different detection systems and other animal species [43].

DISCUSSION AND CONCLUSION

The goal of this thesis was to make a review of non-contact measurement of respiration and cardiac rate. Previously a lot of work has been done in this regard and as discussed earlier.

Monitoring of vital signals can be done with contact using the following different methods: pulse oximeter, ECG, Airflow, spirometry, acoustic, transcutaneous CO2 monitoring, and chest and abdominal movement detection. But also, we can perform this contactless monitoring as developed in our document.

Speaking of contactless methods, several studies have been carried out, the table below gives us a statistical overview of the studies carried out from 2000 to 2020 according to the different methods take on PubMed:

Methods	Numbers of Articles
Ultrasounds sensor	378
Microwave sensor	69
Laser	251
Electromagnetic sensor	288
Infrared/RGB camera	45
IR-UWB	42
Radar	108
Camera based system	170

All these techniques are very useful for monitoring local movements with high resolution, even if the monitored organ is immersed in a dispersive medium. It is shown that the technique is also able to provide reliable results over long periods of time. This provides a useful tool for the detection of malfunctions or diseases in this kind of system and can be used as the basis for the development of experimental models for the study of different types of cardiac and respiratory rate.

On the market, there are different types of sensors commercialize for each of the technics studied. We offer you some images of the sensors found on the market:

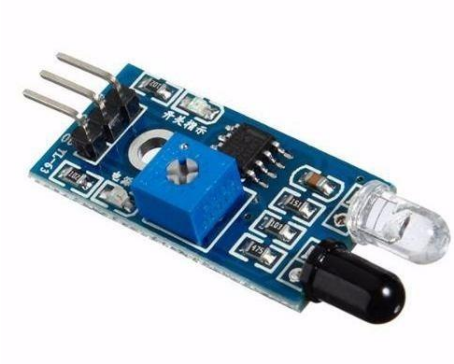

IR sensor

Electromagnetic sensor (HTU21/D315)

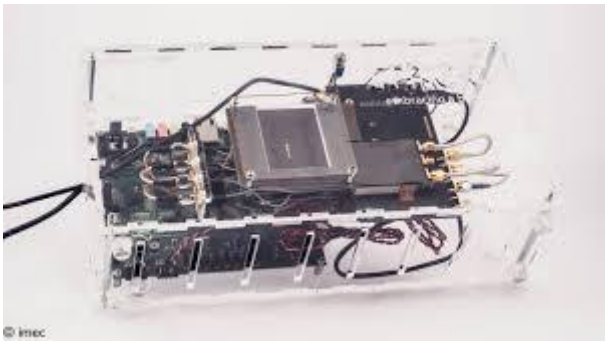

Radar sensor (IMEC)

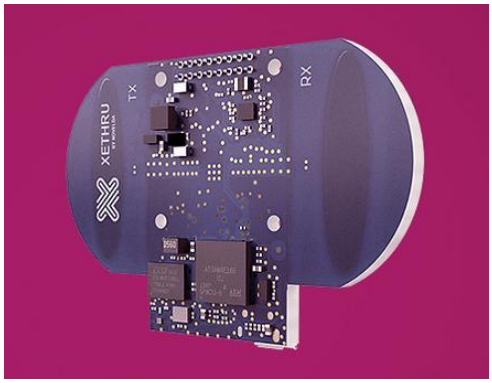

UWB sensor (Novelda AS)

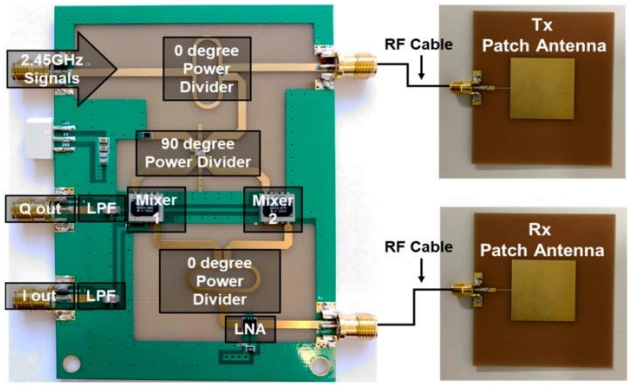

Doppler radar sensor (N5183B)

Prototype for laboratory scale respiration and cardiac monitoring using different sensor has been assembled and tested. Further research could be done in manipulating abnormal respiration and cardiac pattern for case study of diseases. The results will be referred for vital signs telemonitoring system design based on contactless and portable devices.

The results of experiments carried out by non-contact methods compared with contact methods give us practically similar results. the tests being carried out on healthy and sick patients and even simulations on phantoms, which leads us to conclude positively on the monitoring of vital signs without contact.

REFERENCES

[1] ieee sensors journal, vol. 10, no. 11, november 2010

[2] min et al.: noncontact respiration rate measurement system using an ultrasonic proximity sensor.

[3] Khan F, Cho SH. 2017 A detailed algorithm for vital sign monitoring of a stationary/non-stationary human through IR-UWB radar.Sensors (Basel, Switzerland) 17, E290. (doi:10.3390/s17020290)

[4] Khan F, Cho SH. 2017 A detailed algorithm for vital sign monitoring of a stationary/non-stationary human through IR-UWB radar. Sensors (Basel, Switzerland) 17, E290. (doi:10.3390/s17020290)

[5] Hu X, Jin T. 2016 Short-range vital signs sensing based on EEMD and CWT using IR-UWB radar. Sensors (Basel, Switzerland) 16, 2025. (doi:10.3390/s16122025)

[6] royalsocietypublishing.org/journal/rsos R. Soc. open sci. 6: 190149

[7] Lazaro A, Girbau D, Villarino R. 2014 Techniques for clutter suppression in the presence of body movements during the detection of respiratory activity through UWB radars. Sensors (Basel,Switzerland)

[8] Leem SK, Khan F, Cho SH. 2017 Vital sign monitoring and mobile phone usage detection using IR-UWB radar for intended use in car crash prevention. Sensors (Basel, Switzerland)17, E1240. (doi:10.3390/s17061240)

[9] Abdominal wall motion-based respiration rate measurement using an ultrasonic proximity sensor.

[10] Daichi Matsunaga, Shintaro Izumi, Member, IEEE, Keisuke Okuno, Student member, IEEE, Hiroshi Kawaguchi, Member, IEEE, and Masahiko Yoshimoto, Member, IEEE

[11] C. Xianxiang, Xinyu Hu; R. Ren, Z. Bing, T. Xiao, X. Jiabai, F. Zhen, Q. Yangmin, L. Huaiyong and T. Lili, X. Shanhong, “Noninvasive Ambulatory Monitoring of the Electric and Mechanical Function of Heart with a Multifunction Wearable Sensor,” Proc. of IEEE COMPSACW, pp. 662–667, July 2014.

[12] A.K. Tafreshi, M. Karadas, C.B. Top and N.G. Gencer, “Data Acquisition System for Harmonic Motion Microwave Doppler Imaging,” Proc. of IEEE EMBC, pp. 2873–2876, August 2014.

[13] Y. Nakai, S. Izumi, M. Nakano, K. Yamashita, T. Fujii, H. Kawaguchi and M. Yoshimoto, “Noise Tolerant QRS Detection using Template Matching with Short-Term Autocorrelation,” Proc. of IEEE EMBC, pp. 6672–6675, August 2014.

[14] Contact-less Monitoring of Breathing Signal

[15] Respiratory rate 1: why measurement and recording are crucial — Nursing Times.

URL: https: / / www.nursingtimes.net / clinical - archive / respiratory – clinical-archive / respiratory - rate - 1 - why - measurement - and -recording - are - crucial - 26 - 03 – 2018.

[16] F. Q. Al-Khalidi et al. Respiration rate monitoring methods: A review. June 2011. DOI: 10.1002/ppul.21416. URL: http://doi.wiley.com/10.1002/ppul.21416.

[17] Michelle A Cretikos and Rinaldo Bellomo. of Intensive Care and Director of Intensive Care Research 2 Ken Hillman, MB BS, FRCA, FJFICM, Professor of Intensive Care 3 Jack Chen, MB BS, MBA. Tech. rep. 2. 2008. URL: http://www.ncepod.org.uk/2005.htm.

[18] A Novel Non-Contact Heart Rate Monitor Using Impulse-Radio Ultra-Wideband (IR-UWB) Radar Technology

[19] Prgomet, M. et al. Vital signs monitoring on general wards: clinical staff perceptions of current practices and the planned introduction of continuous monitoring technology. Int J Qual Health Care 28, 515–521 (2016).

[20] Liu, Q., Lou, S., Wang, Z. & Li, S. In Microwave and Millimeter Wave Technology (ICMMT), 2016 IEEE International Conference on. 1003–1005 (IEEE).

[21] eger-Madiot, N., Gateau, J., Fink, M. & Ing, R. K. Non-contact and through-clothing measurement of the heart rate using ultrasound vibrocardiography. Med Eng Phys 50, 96–102 (2017).

[22] Giles, D., Draper, N. & Neil, W. Validity of the Polar V800 heart rate monitor to measure RR intervals at rest. Eur J Appl Physiol 116, 563–571 (2016).

[23] Non-Invasive Diagnostic Methods - Image Processing

[24] Allen J. Photoplethysmography and its application in clinical physiological measurement. Physiological Measurement. 2007;28(3): R1-R39

[25] Allen J. Photoplethysmography and its application in clinical physiological measurement. Physiological Measurement. 2007;28(3):R1-R39

[26] Matsui T, Hakozaki Y, Suzuki S, Usui T, Kato T, Hasegawa K, et al. A novel screening method for infl uenza patients using a newly developed non-contact screening system. Journal of Infection. 2010;60(4):271-277. DOI: 10.1016/j.jinf.2010.01.005.

[27] A System for Monitoring Breathing Activity Using an Ultrasonic Radar Detection with Low Power Consumption

[28] Paralax Inc. PING Ultrasonic Distance Sensor; Paralax Inc.: Rocklin, CA, USA, 2006.

[29] Costa, C.; Oliveira, N.; Júnior, E.S.; Melo, P. A noncontact instrument based on ultrasound for the evaluation of asynchronous thoracoabdominal movement in respiratory diseases. In Journal of Physics: Conference Series; IOP Publishing: Bristol, UK, 2018; Volume 1044, p. 012002.

[30] Ali, A.-N.; Javaan, C. Detection of Cardiopulmonary Activity and Related Abnormal Events Using Microsoft Kinect Sensor. Sensors 2018, 18, 920.

[31] Teichmann, D.; Foussier, J.; Leonhardt, S. Respiration monitoring based on magnetic induction using a single coil. In Proceedings of the 2010 IEEE UbiComp Biomedical Circuits and Systems Conference (BioCAS), Paphos, Cyprus, 3–5 November 2010; IEEE: Piscataway, NJ, USA, 2010; pp. 37–40.

[32] Yuan, G.; Drost, N.A.; McIvor, R.A. Respiratory rate and breathing pattern. McMaster Univ. Med. J. 2013, 10, 23–25.

[33] S. Rolfe, "The importance of respiratory rate monitoring," *Br. J. Nurs.*, vol. 28, no. 8, pp. 504–508, Apr. 2019, doi: 10.12968/bjon.2019.28.8.504.

[34] H. Kaneko and J. Horie, "Breathing movements of the chest and abdominal wall in healthy subjects," *Respir. Care*, vol. 57, no. 9, pp. 1442–1451, Sep. 2012, doi: 10.4187/respcare.01655.

[35] A. De Groote, M. Wantier, G. Cheron, M. Estenne, and M. Paiva, "Chest wall motion during tidal breathing," *J. Appl. Physiol.*, vol. 83, no. 5, pp. 1531–1537, 1997, doi: 10.1152/jappl.1997.83.5.1531.

[36] Kramer GH, Capello K, Bearrs B, Lauzon A, Normandeau L. Linear dimensions and volumes of human lungs obtained from ct images. Health physics. 2012; 102(4): 378-383.

[37] Bulletin of Electrical Engineering and Informatics, Vol. 7, No. 1, March 2018, pp. 15~20, ISSN: 2302-9285, DOI: 10.11591/eei.v7i1.711

[38] Sensors 2019, 19, 4778; doi:10.3390/s19214778

[39] stacks.iop.org/MST/14/317

[40] Ivanov P Ch, Rosenblum M G, Peng C K, Mietus J, Havlin S, Stanley H E and Goldberger A L 1996 Scaling behaviour of heartbeat intervals obtained by wavelet-based time-series analysis Nature 383 323

[41] Teich M C, Lowen S B, Jost B M, Vibe-Rheymer K and Heneghan C 2001 Heart rate variability: measures and models, nonlinear biomedical signal processing Dynamic Analysis and Modeling vol 2 (New York: IEEE) ch 6 p 159

[42] Curtis T M, Williamson R and Depledge M H 2000 Simultaneous, long-term monitoring of valve and cardiac activity in the blue mussel Mytilus edulis Marine Biology 136

[43] Mesures sans contact de fonctions vitales : vers une évaluation multisite de l'activité cardiovasculaire